Towards optimal layout design of vertical-axis wind-turbine farms: Double rotor arrangements

Energy Conversion and Management 226 (2020) 113527

Contents lists available at ScienceDirect

Energy Conversion and Management

journal homepage: www.elsevier.com/locate/enconman

Towards optimal layout design of vertical-axis wind-turbine farms: Double rotor arrangements

Sadra Sahebzadeh [a,*], Abdolrahim Rezaeiha [a,b], Hamid Montazeri [a]

[a] Eindhoven University of Technology, Eindhoven, the Netherlands
[b] KU Leuven, Leuven, Belgium

ARTICLE INFO

Keywords:
VAWT
Computational fluid dynamics (CFD)
Wind farm layout design
Wind energy
Power performance
Aerodynamics

ABSTRACT

Designing an optimal wind farm layout requires fundamental knowledge of the interaction of wind turbines in an arrangement. In this paper, extensive high-fidelity CFD simulations are performed to investigate the influence of relative spacing, i.e., distance (R) and angle (Φ), in double rotor arrangements of co-rotating Darrieus H-type vertical axis wind turbines (VAWTs) on their aerodynamic performance. The relative spacing varies within 1.25d $\leq$ R $\leq$ 10d (d: turbine diameter) and $-90° \leq \Phi \leq +90°$. The turbines operate at their optimal tip speed ratio. The analysis is focused on the individual and overall power performance of the turbines and their aerodynamics. Unsteady Reynolds-Averaged Navier-Stokes (URANS) simulations, validated with experiments, are employed. It is found that an optimal region exists in which a higher overall power coefficient ($C_P^{overall}$) compared to the C_P of an isolated solo rotor (C_P^{Solo}) can be achieved. This region corresponds to compact rotor arrangements, i.e. R/d $\leq$ 3d with $\Phi \geq +45°$ and $\Phi \leq -45°$, yielding a maximum 1.8% increment in $C_P^{overall}/C_P^{Solo}$ at R/d = 1.25 and $\Phi = +75°$. Detailed flow analysis reveals that in the optimal spacing, a narrow passage between the two rotors is formed within which the flow accelerates, forming a high-velocity region. The downstream turbine benefits from its blade(s) passing through this region and consequently yields higher C_P values. The findings highlight the high potential for compact VAWT farms with high power density and support the optimal layout design of VAWT farms.

1. Introduction

A wind farm layout design can be improved towards minimizing the wake losses of the turbines [1,2], and consequently, maximizing the overall power output of the farm [3,4]. As a general rule, the larger the spacing between the turbines within a farm, the less the wake losses of the turbines will be [5,6]. However, site constraints limit the available space for wind farms [7,8]. Therefore, an optimal wind farm layout would include the maximum number of turbines per given area with minimum wake losses. Designing an optimal wind farm layout to minimize the wake losses requires fundamental knowledge on the interaction of the wind turbines in an arrangement.

The vast majority of the literature on understanding the wake interactions between the turbines within an arrangement is focused on horizontal axis wind turbines (HAWTs), see for example the review papers by Vermeer et al. [9], Sanderse [10], Sørensen [11], Mehta et al. [12], Shakoor et al. [3], Stevens and Meneveau [13] and Porté-Agel [14]. This is not, however, the case for vertical axis wind turbines (VAWTs). The majority of VAWT studies so far concentrate on isolated turbines, whereas in practice, multiple VAWTs are usually arranged together in a wind farm.

Table 1 presents an overview of the studies on multiple Darrieus VAWTs within an arrangement. The table provides information on the following:

- Method: Previous research has been performed by field measurements, wind-tunnel experiments, low- to moderate-fidelity modeling (e.g., panel/vortex methods), and high-fidelity computational fluid dynamics (CFD) simulations. The majority of these studies used CFD simulations in which the Unsteady Reynolds-Averaged Navier-Stokes (URANS) approach has been widely employed.
- Number of rotors: As the research on the layout design of VAWT farms is still at a very early stage, the majority of the studies are mostly focused on the most fundamental arrangement, i.e., the double rotor arrangement. This arrangement is also the focus of the present study.

* Corresponding author at: Eindhoven University of Technology, Eindhoven, the Netherlands.
E-mail address: s.sahebzadeh@tue.nl (S. Sahebzadeh).

https://doi.org/10.1016/j.enconman.2020.113527
Received 6 July 2020; Received in revised form 8 October 2020; Accepted 9 October 2020
Available online 9 November 2020

Nomenclature

A	Turbine swept area, $H.d$ [m^2]	R	Relative distance of the turbines [m]
c	Airfoil chord length [m]	Re_c	Chord-based Reynolds number, $cU_\infty\sqrt{1+\lambda^2}/\nu$ [−]
C_m	Instantaneous moment coefficient [−]	U	Time-averaged velocity magnitude [m/s]
C_P	Power coefficient [−]	U_∞	Freestream velocity [m/s]
d	Turbine diameter [m]	Δθ	Phase lag between the two turbines [°]
W	Domain width [m]	λ	Tip speed ratio, $\Omega d/2U_\infty$ [−]
dθ	Azimuthal increment [°]	ν	Kinematic viscosity [m^2/s]
M	Moment [Nm]	θ	Azimuthal angle [°]
H	Turbine height [m]	q	Dynamic pressure [Pa]
n	Number of blades [−]	σ	Solidity, nc/d[−]
		Φ	Relative angle of the turbines [°]
		Ω	Rotational speed [rad/s]

Table 1
Overview of the studies on Darrieus VAWT farms.

Authors (date)	Method	No. of rotors	Studied parameters	No. of arrangements (No. of cases)	Focus of study
Dabiri (2011) [4]	FM	6	R, Φ, RD	11 (11)	C_P
Brownstein et al. (2016) [15]	LF (LRB)	2, 4, 10, 18, 24	R, Φ	20 (20)	C_P, Wake
Zanforlin & Nishino. (2016) [5]	CFD (URANS)	2	R, Φ, RD, WD, λ	2 (24)	C_P, Wake
Ahmadi-Baloutaki et al. (2016) [16]	WT	2, 3	R, RD	7 (7)	Wake
Lam & Peng. (2017) [17]	WT	2	RD	1 (3)	Wake
Chen et al. (2017) [18]	CFD (DES)	2	WD, λ, R, Φ, RD, Δθ	4 (16)	C_P, Wake
Tavernier et al. (2018) [19]	LF (P/V)	2	λ, σ, Φ, WD	1 (5)	C_P, Wake
Barnes & Hughes (2018) [20]	CFD (URANS)	5, 6, 9, 15, 16	R, Φ	5 (5)	C_P, Wake
Alexander & Santhanakrishnan. (2019) [21]	CFD (URANS)	2	RD	1 (2)	C_P, Wake
Brownstein et al. (2019) [6]	WT	2	R, Φ, WD	5 (5)	C_P, Wake
Peng et al. (2020) [22]	CFD (URANS)	2	AF, PA, σ, RD, R	4 (16)	C_P

FM = field measurement, **LF** = low fidelity, **LRB** = Leaky-Rankine body, **CFD** = computational fluid dynamics, **URANS** = unsteady Reynolds-Averaged Navier-Stokes, **WT** = wind-tunnel measurement, **P/V** = panel/vortex method, **R** = relative distance, **Φ** = relative angle, **RD** = rotation direction, **WD** = wind direction, **λ** = tip speed ratio, **Δθ** = phase lag, **σ** = solidity, **AF** = airfoil type, **PA** = pitch angle.

- Studied parameters: Previous studies have mainly focused on investigating the impact of relative distance (R) and angle (Φ) of the turbines, rotational direction of the turbines and their phase difference. In addition, the impact of tip speed ratio and solidity has also been studied in a few works. The present study is focused on the impact of R and Φ, as the most influential parameters, at the optimal tip speed ratio.
- Number of arrangements: The number of investigated arrangements has been rather limited, with a maximum number of 20, which would not be sufficient to provide a comprehensive map on the power performance of a multi-rotor VAWT farm and to specify the optimal arrangement(s). In the present study, a total number of 119 arrangements (7 relative distances and 17 relative angles) are investigated to provide a high-resolution map of the power performance of the double rotor arrangements of VAWTs.
- Focus of study: In previous studies, the power performance and/or the wake of the rotors in the arrangement have been investigated. In the present study, the individual and overall power performance, wake characteristics and blade aerodynamics are investigated for two vertical axis wind turbines (VAWTs) in a double rotor arrangement.

The conclusions of the literature on multiple VAWT wake interactions suggests a potential for power gain for adjacent VAWTs within a farm due to some synergic wake interactions. Following a series of field measurements, Dabiri [4] and Whittlesey et al. [23] concluded that in certain layouts, VAWT farms have the potential to reach an order of magnitude higher power densities compared to HAWT farms. Peng et al. [22] and Alexander and Santhanakrishnan [21] predicted a power gain increase of 8–13% in specific operating conditions and arrangements, thought to be due to the discussed synergic interactions. Zanforlin and Nishino [5] and Bremseth and Duraisamy [24] found that this power increase could be due to the contraction of the wake of the turbines and development of regions of excess momentum between the turbines. Benefitting from the discussed potential, VAWT farm layout(s) could be designed with higher wind farm power density (i.e., wind farm generated power over the farm area [25]), up to 50–100% [24]. This would be very promising. However, further research is still needed to more comprehensively solidify this potential and elucidate in more detail the arrangements which can realize this potential. This is essential because:

1. The conclusions presented by the literature, although valuable, are based on a limited number of VAWT arrangements. A wide range of potential power gain for adjacent VAWTs is reported in the literature ranging from 8% [22] up to 100% [24] and there is little consensus on the extent of this potential;
2. Optimal regions for placing subsequent rotors in VAWT arrangements are not well identified;
3. An overall performance map cannot be generated for VAWT arrangements based on the existing literature;
4. Mechanisms leading to power performance enhancement and C_P increment of VAWT arrangements are not yet fully understood.

Table 2
Details of the test cases.

Relative distance (R) [−]	1.25d, 1.5d, 1.75d, 2.25d, 3d, 5d, 10d
Relative angle (Φ) [°]	0°, ±5°, ±10°, ±15°, ±30°, ±45°, ±60°, ±75°, ±90°

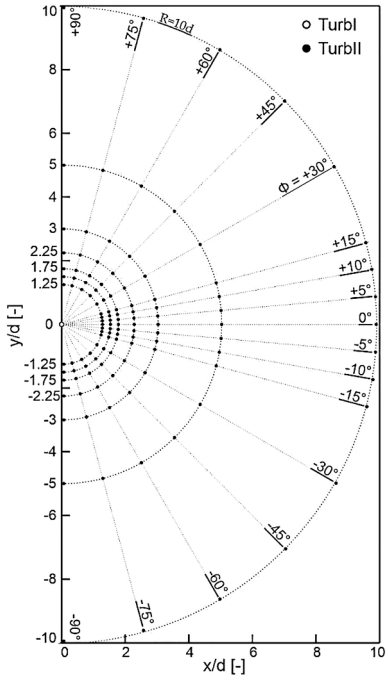

Fig. 1. Schematic of the studied double rotor arrangements (119 unique arrangements in total). White circle indicates TurbI and black circles indicate the position of TurbII.

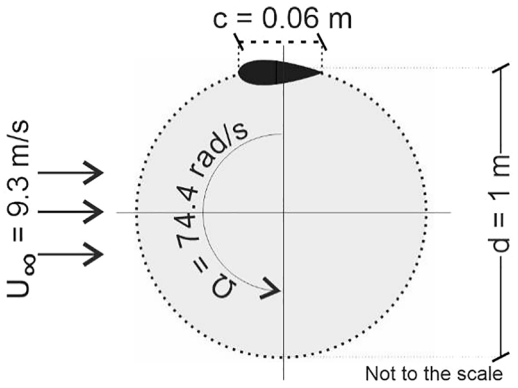

Fig. 2. Schematic of the turbines (TurbI, TurbII, and solo turbine).

Table 3
Geometrical and operational characteristics of the turbines (TurbI, TurbII, and solo turbine).

Parameter	Value
Number of blades, n [−]	1
Diameter, d [m]	1
Height, H [m]	1
Swept area, A [m^2]	1
Solidity, σ [−]	0.06
Airfoil chord length, c [m]	0.06
Airfoil shape [−]	NACA0018
Rotational speed, Ω [rad/s]	74.4
Freestream velocity, U_∞ [m/s]	9.3
Tip speed ratio (based on U_∞), λ [−]	4
Turbulent intensity, TI [%]	5
Chord-based Reynolds number, Re_c [−]	1.57×10^5

The present paper, therefore, aims to address these gaps by providing insight into the power performance and wake interactions of VAWTs in a double rotor arrangement, as the smallest generating cell in wind farms. The objectives of the work are as follows:

1. Providing generalizable conclusions by developing a high-resolution power performance matrix with a large number of possible arrangements and minimum interpolation, covering a wide range of the relative angles and distances.
2. Identification of optimal arrangements of the array;
3. Developing a map for the power performance of individual turbines and the overall arrangement as a function of the relative spacing of the turbines;
4. Identification of aerodynamic mechanisms that contribute to the power performance enhancement/reduction of the individual turbines and consequently, the overall arrangement.

To obtain these objectives, an extensive number of high-fidelity URANS simulations, validated with experimental data, are performed to investigate the influence of relative spacing, i.e., distance (R) and angle (Φ), in double rotor arrangements of co-rotating Darrieus H-type vertical axis wind turbines (VAWTs) on their aerodynamic performance. In total, 119 arrangements of the turbines are investigated.

It is believed that by obtaining the aforementioned objectives, the potential for compact VAWT farms with high power density will be further clarified, and further understanding towards optimal layout design of VAWT farms will be developed. This can also be highly beneficial in the design of urban and building-integrated VAWT farms where the available space for the installation of wind energy harvesting systems may be limited. Furthermore, the overall output of the arrangement averaged over all wind directions as a function of the relative distance is quantified. This can be especially beneficial in urban farms experiencing frequent changes in wind direction.

The rest of the paper is organized as follows: Test cases are introduced in Section 2. Sections 3.1–3.3 detail the geometrical and operational characteristics of the turbines, computational domain and grid, solver settings and boundary conditions, respectively. Solution verification and validation are presented in Section 3.4. The results, including analysis of the power performance are presented in Section 4, followed by aerodynamics divided into two subsections of 5.1. Near wake and blade aerodynamics and 5.2. Far wake. Discussion and conclusions follow in Sections 6 and 7, respectively.

2. Test cases

The analysis is performed for an array of two co-rotating Darrieus H-type VAWTs with zero phase lag in 119 different arrangements: 7 relative distances (R), ranging from 1.25d to 10d (d: turbine diameter), and 17 relative angles (Φ), ranging from −90° to + 90°, see Table 2. Fig. 1 illustrates a schematic of the studied arrangements for the double rotor array.

The choice of 10d as the upper limit of relative distances is based on the prior knowledge from the literature on the approximate wake length of a similar turbine at the same operating condition [26].

To set a baseline for comparison, a solo turbine with the same geometrical and operational characteristics is also considered.

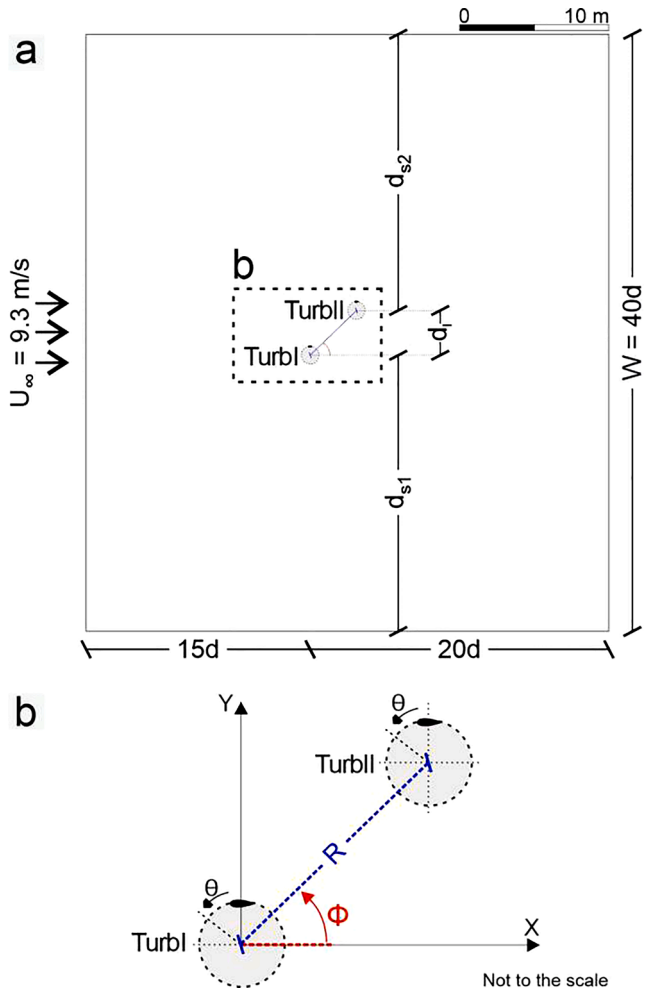

Fig. 3. (a) Computational domain and (b) schematic of computational domain with R (relative distance) and Φ (relative angle) indicated.

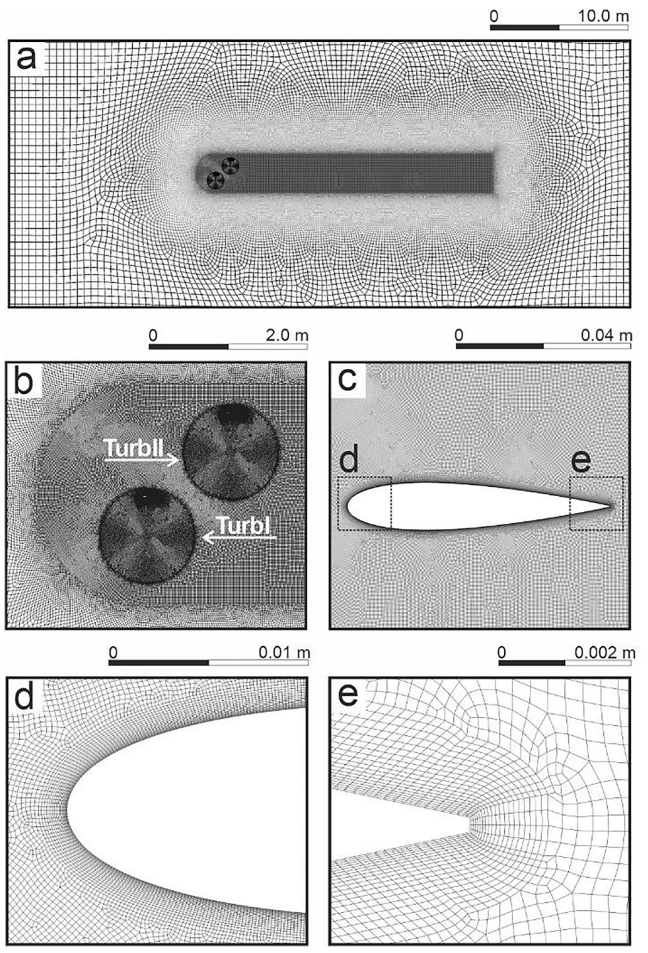

Fig. 4. Computational grid for a sample double rotor arrangement (R = 1.25d and Φ = +45°). Note that sub-figure a is a cropped portion of the whole domain.

3. CFD simulations

3.1. Turbine geometrical and operational characteristics

The simulated turbines are single-straight-bladed Darrieus H-type VAWTs, schematically depicted in Fig. 2. The geometrical and operational parameters of the two identical turbines are provided in Table 3. The turbines are selected with respect to the wind-tunnel study by Tescione et al. [27], which is also employed for the validation study (see Section 3.4). Note that considering the computational costs and the numerous transient simulations performed in the present study, the turbines are simplified to only include one blade. Nevertheless, based on the conclusions of Ref. [28], the aerodynamic performance and the wake of the low-solidity VAWTs operating within the optimal regime are marginally affected by the number of blades. This simplification, therefore, is expected to have minimal impact on the conclusions of the present study. The location of the blade-strut connection is at mid-chord. In order to reduce the computational costs, the turbine is simplified by excluding the shaft and the connecting rods from the geometry. Also note that earlier studies have shown that these less-aerodynamic bodies result in a systematic drop in the turbine power performance, e.g., Ref. [29,30]. Therefore, neglecting these components is not expected to significantly influence the conclusions of this study.

3.2. Computational domain and grid

Considering the large number of simulations and to reduce the computational costs, a two-dimensional computational domain, consisting of two co-rotating cores and a fixed surrounding domain is used. Note that the use of the two-dimensional domain is accordant with findings of Rezaeiha et al. [31,32] in which a systematic difference between the results of the 2D and 2.5D computational domains was observed. The relative distance (R) of the two turbines is defined as the length of the turbines' center-to-center line. The relative angle of the two turbines (Φ) is defined as the angle between the turbines' center-to-center line and the x-axis (Fig. 3). Relative spacing is, therefore, the combination of R and Φ.

Domain size is 35d × 40d (width × length), selected based on the best-practice guidelines for VAWT CFD simulations [31,32]. For all the simulations, there is a 15d distance between the upstream turbine's center and the domain inlet. In addition, there is a minimum distance of 10d between the downstream turbine and the domain outlet. To guarantee the same distance between the symmetric side-boundaries and the upstream and downstream turbines, the longitudinal axis of the domain passes through the middle of the lateral distance of the two rotors (d_l). In other words, in all the simulations, $d_{s1} = d_{s2}$. Furthermore, a minimum distance of 10d from the boundary sides of the domain is considered in all cases ($d_{s1} = d_{s2} > 10d$). The 2D blockage ratio for the double rotor

Table 4
Grid-sensitivity analysis details for a sample case (R = 1.25d and Φ = 0°).

Grid	Number of cells	Number of cells along the airfoil	Maximum y^+
Coarse	414,096	565	5.7
Medium	745,422	800	3.8
Fine	1,381,353	1130	2.7

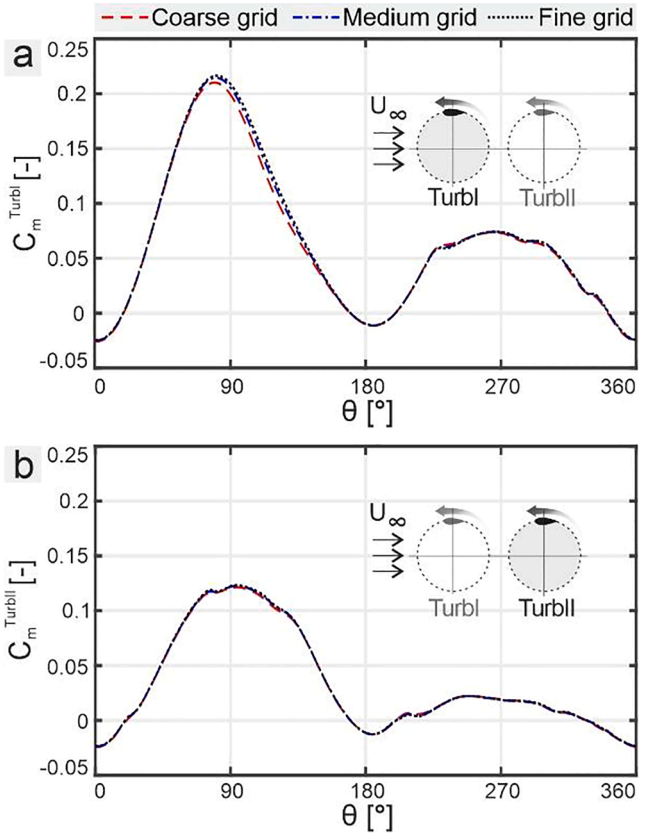

Fig. 5. Grid-sensitivity analysis: instantaneous moment coefficient (C_m) for (a) TurbI and (b) TurbII for three grids.

array $\left(\frac{2d}{W}\right)$ is ≤ 5%.

Fig. 4 illustrates the computational grid for a sample case (R = 1.25d and Φ = +45°), which consists of ≈0.8 million quadrilateral cells. Considering the different arrangements, the number of cells ranges from ≈0.7 to ≈1.4 million cells. The maximum and average y^+ on the turbines blade is 4.2 and <1.8 for all cases, respectively, with 800 cells along the blade circumference.

For the solo turbine a domain with the same blockage ratio as the double rotor arrangements is made. In this case, the computational grid consists of ≈0.5 million quadrilateral cells. The maximum and average y^+ values for the solo turbine are 4.1 and 1.7, respectively.

3.3. Solver settings and boundary conditions

Incompressible unsteady Reynolds-averaged Navier-Stokes (URANS) equations are solved using the commercial CFD software package ANSYS Fluent 19.1 [33]. The SIMPLE scheme is used for pressure–velocity coupling [34,35]. Second-order upwind discretization is employed both in time and space using a 4-stage Runge-Kutta scheme [36]. Regarding the time-advancement scheme, a (global) constant time-stepping is used.

Turbulence is modeled using the 4-equation transition SST (γ-Re_θ) turbulence model [37]. The transition SST model solves two additional transport equations for intermittency (γ) and momentum-thickness Reynolds number (Re_θ) together with the two transport equations of the widely-used SST k- ω model [38] to account for laminar-to-turbulent transition. In addition, the production limiters by Menter [39] and Kato [40] are used to limit the turbulence production in the stagnation regions. Furthermore, curvature correction, a modification to the turbulence production term, is employed to sensitize the turbulence model to the effects of streamline curvature and system rotation [41].

Following the best practice guidelines [31,32], all simulations are performed with the same azimuthal increment of dθ = 0.1° and 20 iterations per time-step. The number of turbine revolution to reach statistical convergence is 20 and all the presented results are sampled at the 21st revolution of the turbines.

The sliding grid technique [42] is used for the interface between the rotating cores and the fixed domain. The boundary conditions at the inlet, outlet, side faces and blade walls are: uniform streamwise mean velocity, zero static gauge pressure, symmetry and no-slip wall, respectively. A freestream velocity of U_∞ = 9.3 m/s with a turbulence intensity of 5% is set at the inlet while the incident flow turbulence intensity is 3.65% due to the decay in the domain [31,43]. Note that the incident value is defined as the value that would occur at the location of the turbine, if the turbine would be absent [44,45]. The transient simulation is initialized with the results of a steady RANS simulation with blades fixed at θ = 0°. The turbulence length scale is 1 m (=d). The computational settings are based on the best-practice guidelines for accurate CFD simulation of VAWTs [28,31,32,46,47].

Table 5
Power coefficient of upstream turbine (C_P^{TurbI}), downstream turbine (C_P^{TurbII}), and overall value ($C_P^{Overall}$), calculated using the three grids.

Parameter	Grid		
	Coarse	Medium	Fine
C_P^{TurbI}	0.251	0.259	0.263
C_P^{TurbII}	0.132	0.134	0.135
$C_P^{Overall}$	0.192	0.196	0.199

3.4. Solution verification and validation

In order to investigate the dependency of the results on the grid resolution, a detailed grid-sensitivity analysis is performed. Three uniformly-refined grids with a linear refinement factor of $\sqrt{2}$ are employed for a sample case with R = 1.25d and Φ = 0°. The details of the grids are given in Table 4.

Fig. 5 shows the instantaneous moment coefficients (C_m) for the two

Table 6
Comparison of the CFD against experimental data for the three validation studies.

Comparison of CFD result with experimental data by Ferreira et al. [49]						
θ [°]	90	108	133	158	223	
Absolute deviation of the strength of the circulation of leading-edge vortex [%]	31.1	11.6	4.5	16.6	7.4	
Comparison of CFD result with experimental data by Tescione et al. [27]						
X/R	1.5	2	2.5	3	3.5	4
Average deviation of streamwise velocity [%]	6.8	8.0	9.8	11.7	12.3	16.0
Average deviation of lateral velocity [%]	2.8	2.5	2.3	2.2	2.3	2.8
Comparison of CFD result with experimental data by Castelli et al. [50]						
λ	2.04	2.33	2.51	2.64		3.08
Absolute deviation of C_P [%]	3.42	10.7	0.5	6.8		23.2

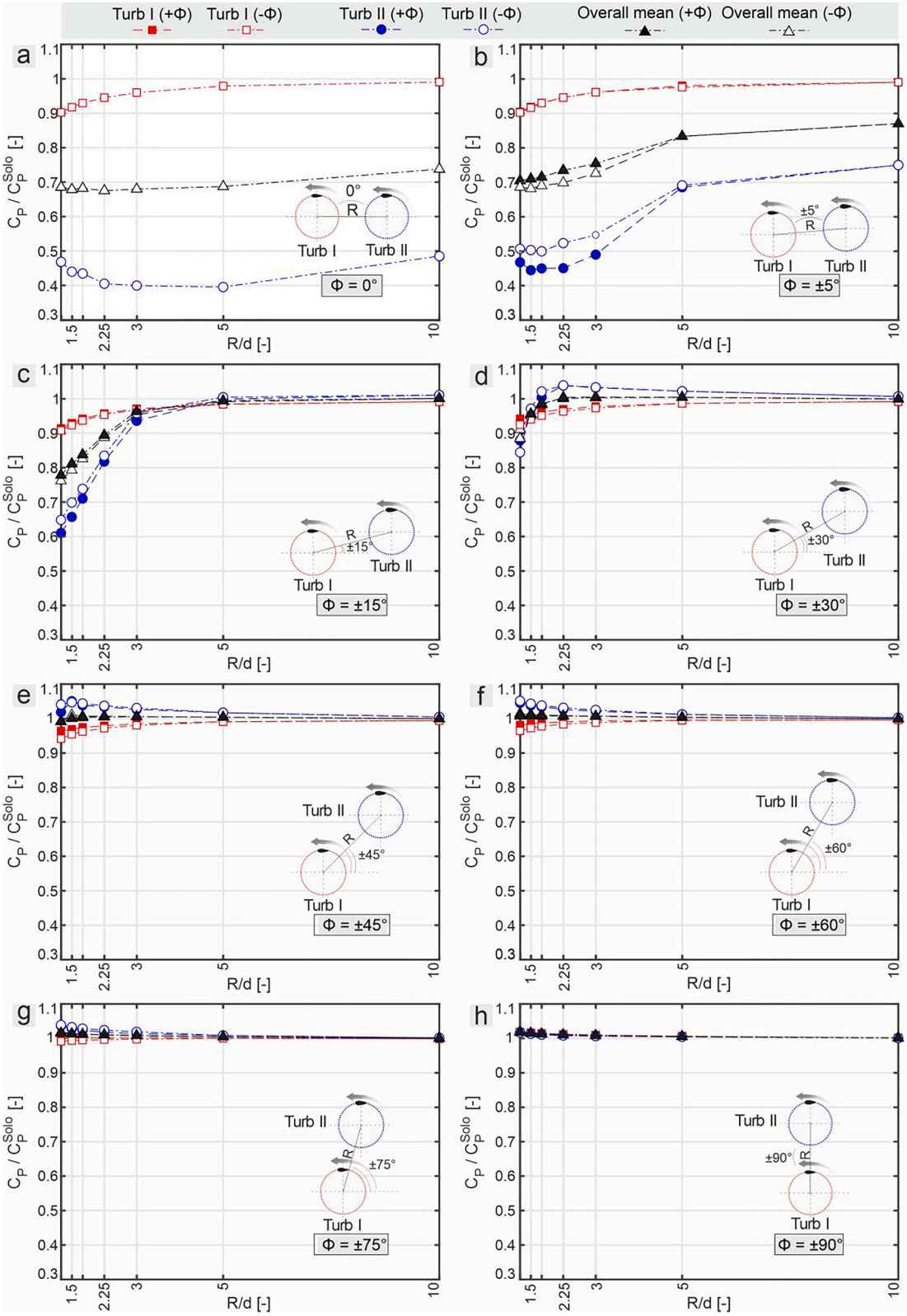

Fig. 6. Effect of relative distance (R) on individual and overall power performance of the turbines for different relative angles (Φ).

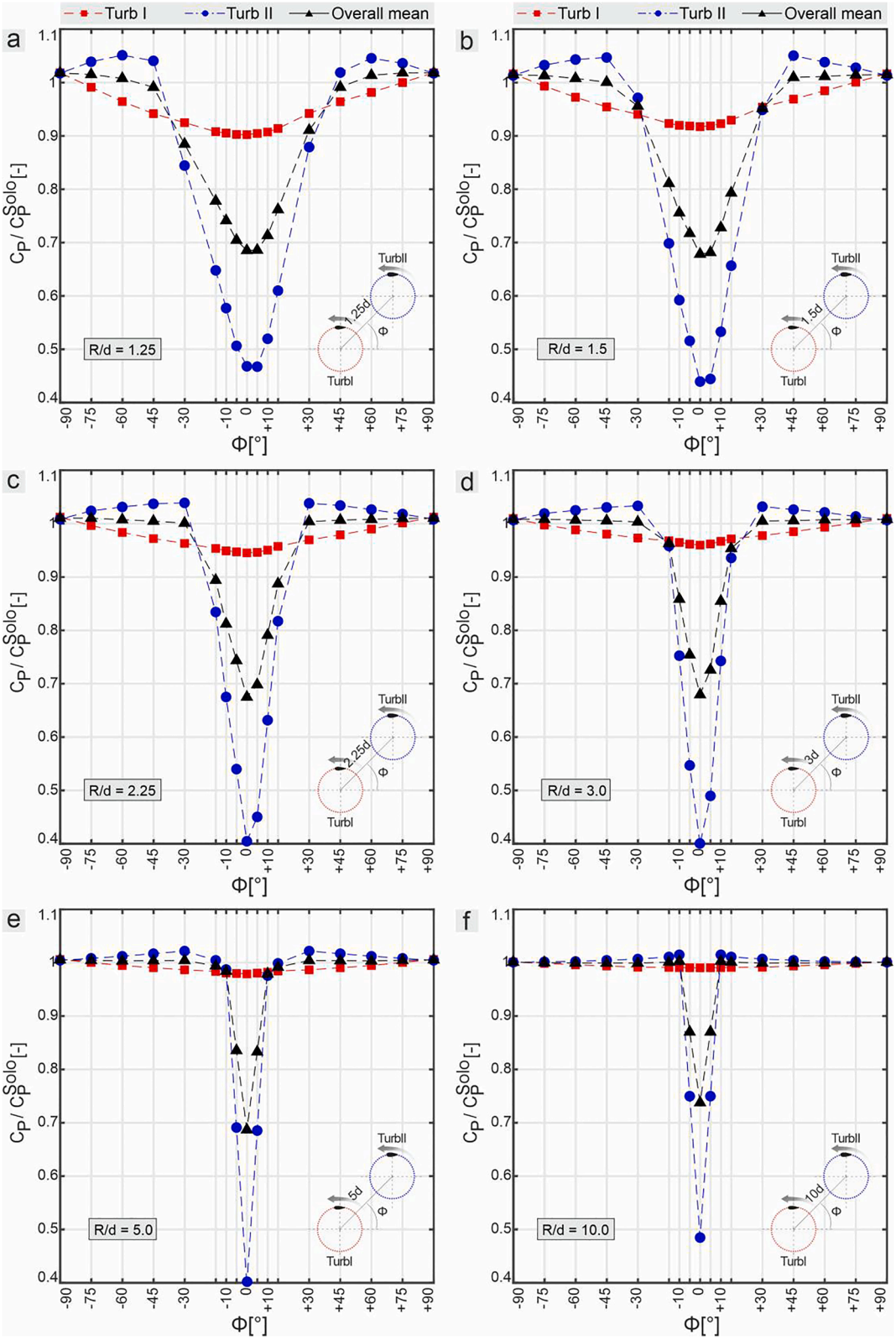

Fig. 7. Effect of relative angle (Φ) on individual and overall power performance of the turbines for different relative distances (R).

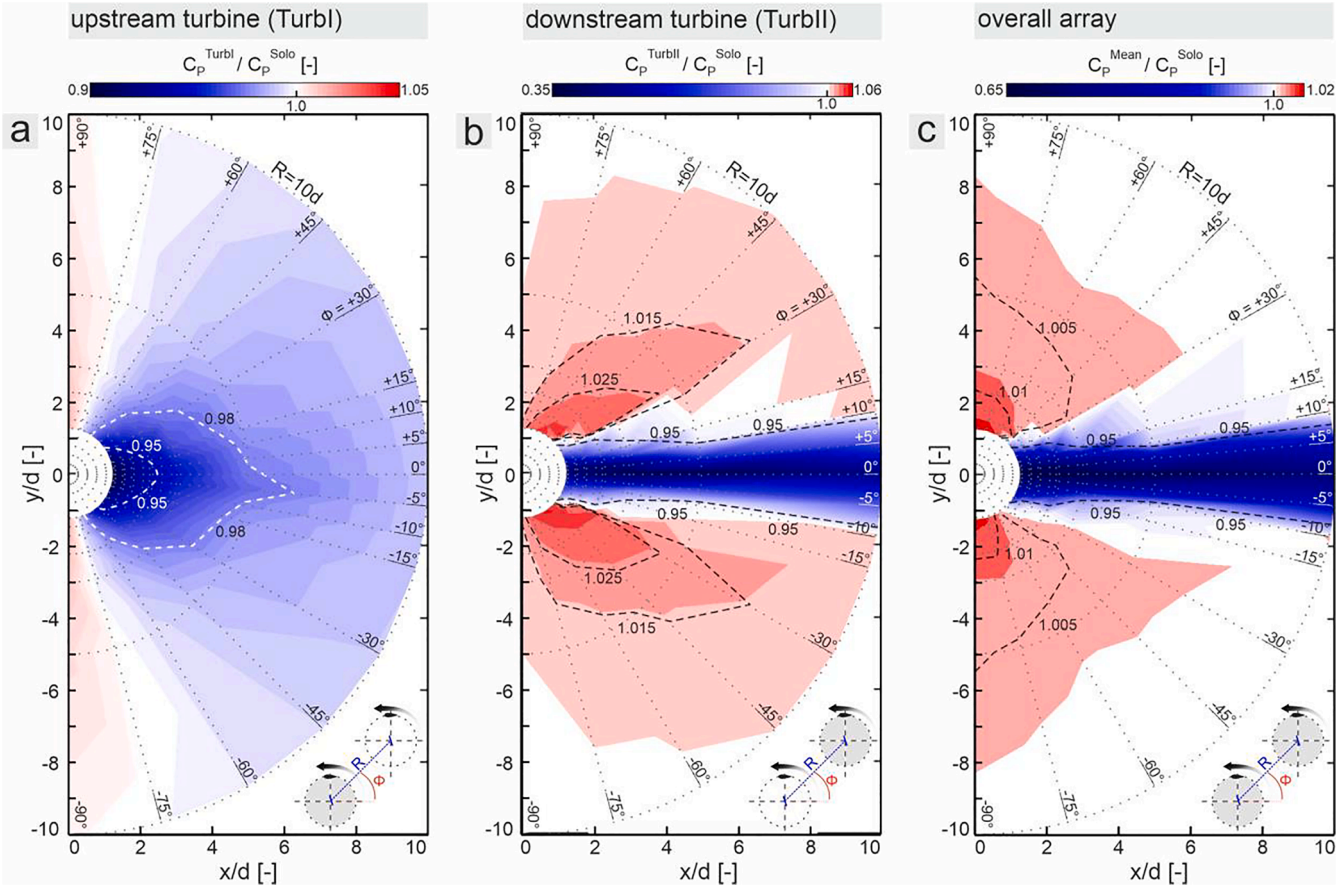

Fig. 8. Contour plots of the power performance of (a) the upstream turbine (TurbI), (b) downstream turbine (TurbII), and (c) overall array in R-Φ space (Note the difference in the colorbars).

turbines, calculated using the three uniformly refined grids. Negligible differences between the three C_m curves are observed for both turbines and the lines corresponding to the medium and fine grids are almost overlapping.

The C_P values for the three grids are reported in Table 5. The power coefficient of each individual turbine is calculated using Eq. (1):

$$C_P = \frac{M\Omega}{qU_\infty A} \tag{1}$$

The overall power coefficient of the array is defined as the arithmetic mean of the individual power coefficient of TurbI (C_P^{TurbI}) and TurbII (C_P^{TurbII}) using Eq. (2):

$$C_P^{Overall} = \frac{C_P^{TurbI} + C_P^{TurbII}}{2} \tag{2}$$

The difference in C_P values between the fine-medium and medium-coarse grid pairs for the upstream turbine is 1.5% and 3%, respectively. This is 0.7% and 1% for the downstream turbine, and 1.2% and 2.3% for the overall C_P of the arrangement, respectively. The grid convergence index (GCI) [48] is also calculated using the overall C_P values with a safety factor (F_s) of 1.25. The GCI^{coarse} and GCI^{fine} values for the medium-fine grid pair are 3.2×10^{-3} and 2.4×10^{-3}, respectively, corresponding to 1.6% and 1.2% of the exact overall C_P value calculated using the Richardson extrapolation.

In addition, to make sure of the suitability of the grid for the study of the wake, dimensionless time-averaged lateral and streamwise velocities are compared along three lines at the lateral direction: X/d = 0.625, 2 and 4 for the three grids. Negligible differences are observed where the overall deviation along the three lines is <1%. Based on this analysis, the medium grid is chosen for the rest of the study.

Three separate validation studies have been previously performed, where the CFD simulations are compared with measurements of three different wind tunnel experiments for solo Darrius H-type VAWTs in different operational regimes. Since these validation studies have been published as separate papers [46,47], a brief description of the three experiments and the validation studies is given below. A comparison of the CFD results and the experimental data is given in Table 6.

I. Wind-tunnel experiments by Ferreira et al. [49] were carried out in a low-turbulence wind tunnel. The blade aerodynamics of a one-bladed rotor was studied using 2D particle image velocimetry (PIV) in different conditions. The evolution of the flow around the blade is analyzed with a particular focus on the leading-edge separation vortex and trailing edge shed vorticity. In this validation study, the vorticity field and the characteristics of the separated/shed leading-edge vortex for the turbine blade in dynamic stall is compared against the experimental data. A reasonably good agreement between the wind tunnel results and the CFD results is achieved. For the azimuthal angles of $\theta = 108^\circ$, 133° and 223°, the absolute deviations between the measured and simulated strength of the circulation of the leading-edge vortex are 4.5%, 7.4% and 11.6%, respectively (Table 6).
II. Wind-tunnel experiments by Tescione et al. [27] were carried out in the open-jet facility, TU Delft. Stereoscopic PIV measurements

Table 7
Normalized C_P values (averaged over Φ) for the individual turbines and the overall array.

R/d [−]	1.25	1.5	1.75	2.25	3	5	10
C_P^{TurbI}/C_P^{Solo}, averaged over Φ	0.95	0.96	0.96	0.97	0.98	0.99	0.99
C_P^{TurbII}/C_P^{Solo}, averaged over Φ	0.81	0.83	0.84	0.86	0.88	0.93	0.95
$C_P^{Overall}/C_P^{Solo}$, averaged over Φ	0.88	0.89	0.90	0.92	0.93	0.96	0.97

were acquired at the mid-span of a two-bladed rotor to study the turbine near wake. In this validation study, the measured and computed time-averaged normalized streamwise and lateral velocity components are compared along lines at different streamwise positions in the turbine wake (Table 6). For the streamwise and lateral velocity component, the maximum deviations are 16% and 2.8%, respectively, which occur along line X/R = 4 (Table 6).

III. Wind-tunnel experiments by Castelli et al. [50] were carried out in a low-turbulence wind tunnel, measuring torque and rotational speed of a three-bladed rotor. The turbine power curve was calculated for a range of conditions. In this validation study, the turbine power coefficient (C_P) at different tip speed ratios is compared against the experimental data. As shown in Table 6, a good agreement between CFD and experiment is observed. The absolute deviation between the simulated and measured C_P is about 0.5%, 3.4%, and 6.8% for λ = 2.51, 2.04, and 2.64, respectively.

Table 8
Individual and overall power coefficients (C_P) of the turbines in the selected arrangements.

Sample arrangement (R = 1.5d)	C_P^{TurbI}/C_P^{Solo}	C_P^{TurbII}/C_P^{Solo}	$C_P^{Overall}/C_P^{Solo}$
Φ = 0°	0.917	0.440	0.679
Φ = +15°	0.930	0.657	0.793
Φ = +30°	0.954	0.949	0.951
Φ = +45°	0.969	1.051	1.01
Φ = +90°	1.016	1.013	1.015

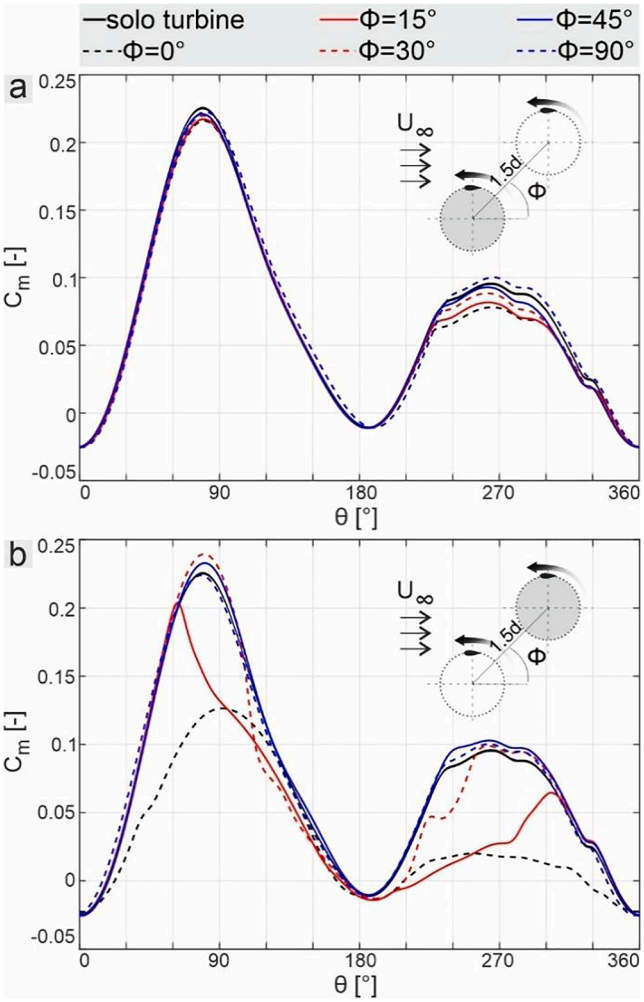

Fig. 9. Instantaneous momentum coefficient (C_m) for (a) the upstream and (b) downstream turbines in the selected arrangements (R = 1.5d).

These three sets of validation studies with different geometrical and operational characteristics and different measured parameters confirm the validity of the numerical modeling approach for CFD simulations of VAWTs. Further details of the validation studies are presented Refs. [46,47].

4. Power performance

4.1. Solo rotor

The predicted power coefficient for the solo rotor, C_P^{Solo}, is 0.287. This value is used in the rest of the paper for normalization.

4.2. Double rotor array

Figs. 6 and 7 present the effect of relative distance (R) and angle (Φ) on the individual and overall power performance of the two rotors in the array, respectively. Fig. 8 shows the contour plots of the C_P of the upstream turbine (TurbI), downstream turbine (TurbII), and the overall array in the R-Φ space. The following observations are made for the upstream rotor (Section 4.2.1), downstream rotor (Section 4.2.2), and the overall array (Section 4.2.3):

4.2.1. Upstream turbine (TurbI)

The power performance of TurbI is influenced by the induction of the downstream turbine. For the studied range of Φ and R, C_P^{TurbI} drops to a minimum of 90% of C_P^{Solo} for R/d ≤ 2.25 at $-45° \le \Phi \le +30°$. This is in line with the findings of Tavernier et al. [19], who predicted a similar drop in the power performance of the upstream turbine. In that study, however, the range of Φ for which this drop occurs is larger. This is likely due to the smaller number of the studied arrangements. Note that the asymmetry in Φ highlights more extensive induction on the leeward side. The asymmetry has also been reported in the wind-tunnel measurements by Brownstein et al. [6]. Outside this region (shown with a dashed white line in Fig. 8a), the impact of TurbII on C_P^{TurbI} is limited to <5%, while this is below 2% for R/d ≥ 5.

4.2.2. Downstream turbine (TurbII)

The observations regarding the power performance of the downstream turbine (C_P^{TurbII}) are presented for the following three identified regions: (i) wake, (ii) optimal, and (iii) minimal interaction regions. It should be noted that dashed lines are included in Fig. 8b to roughly represent the three regions.

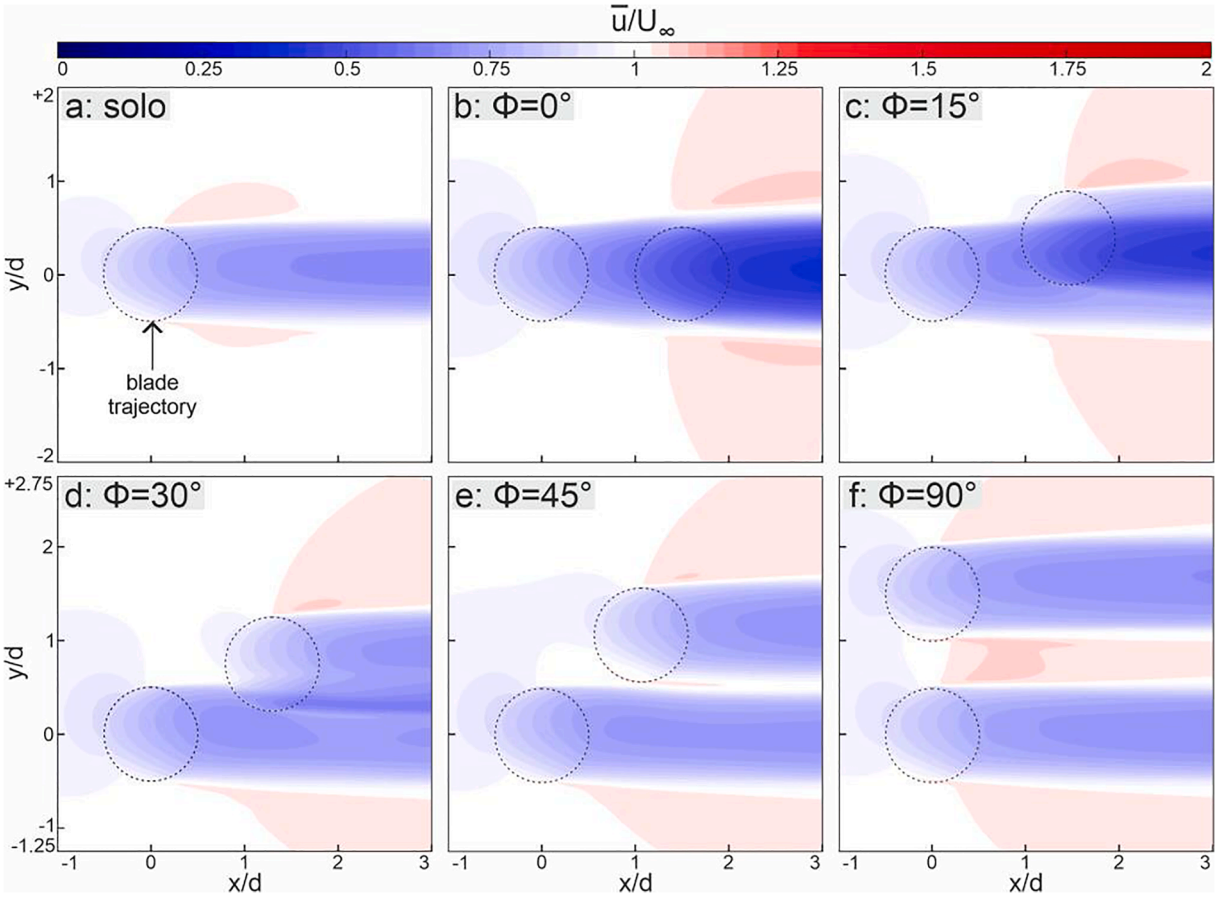

Fig. 10. Normalized time-averaged (over one turbine revolution) streamwise velocity for solo rotor and double rotor arrangements with R = 1.5d for different relative angles.

(i) *Wake region:* This region is defined as the range of R and Φ in which $C_P^{TurbII}/C_P^{Solo} < 0.95$, corresponding to a significant drop in C_P^{TurbII} due to the presence in the wake of the upstream turbine. The region includes the following relative spacing ranges:

a) $-5^\circ \leq \Phi \leq +5^\circ$ with $R/d \leq 10$;
b) $-15^\circ \leq \Phi < -5^\circ$, $+5^\circ < \Phi \leq +15^\circ$ with $R/d \leq 3$;
c) $-30^\circ \leq \Phi < -15^\circ$, $+15^\circ < \Phi \leq +30^\circ$ with $R/d \leq 1.5$;

In sub-region (a), the reduction in C_P^{TurbII} is most significant with a minimum value of 39.5% of C_P^{Solo}, which occurs at $R/d = 5$ and $\Phi = 0^\circ$. Further downstream, the wake recovery starts and C_P^{TurbII} increases to 48.5% of C_P^{Solo} at $R/d = 10$ and $\Phi = 0^\circ$. In sub-region (b), the reduction in C_P^{TurbII} is less extensive and it extends only to the farthest downstream distance of $R/d = 3$, limited to a minimum value of 52% of C_P^{Solo} at the small relative distance of $R/d = 1.25$. In sub-region (c), the minimum C_P^{TurbII} is 84.5% of C_P^{Solo}.

(ii) *Optimal region:* This region is defined as the range of R and Φ in which $C_P^{TurbII}/C_P^{Solo} \geq 1.025$. Within this region, the power performance of TurbII is slightly higher than C_P^{Solo} due to synergic interactions between the two turbines. The region includes the following relative spacing ranges:

a) $\Phi = \pm 30^\circ$ with $2.25 \leq R/d \leq 3$;
b) $\Phi = -45^\circ$ with $1.25 \leq R/d \leq 3$; $\Phi = +45^\circ$ with $1.5 \leq R/d \leq 3$;
c) $\Phi = -60^\circ$ with $1.25 \leq R/d \leq 3$; $\Phi = +60^\circ$ with $1.25 \leq R/d \leq 2.25$;
d) $\Phi = -75^\circ$ with $1.25 \leq R/d \leq 1.75$; $\Phi = +75^\circ$ with $1.25 \leq R/d \leq 1.5$;

Within this region, C_P^{TurbII} values of 5.1% and 5.2% higher than C_P^{Solo} are observed at $R/d = 1.5$, $\Phi = +45^\circ$ and $R/d = 1.25$, $\Phi = -60^\circ$, respectively. This is in line with the findings of Tavernier et al. [19] and Dabiri [4]. In those studies, which have been performed in a λ value close to the current study, a similar range of values for C_P^{TurbII} increment was reported. The field measurements by Dabiri [4] also identified the range $+30 < \Phi < +45^\circ$ as the optimal relative angle for two adjacent rotors in a relative distance close to $R/d = 1.5$. By increasing the value of Φ from -45° to -75°, the radial extent of the optimal region decreases from 3d to 1.75d. This proposes that a higher relative angle allows for a more compact optimal spacing in the arrangement. It should be noted that Tavernier et al. [19] identified a larger optimal region for the downstream turbine. The difference could be due to the lower fidelity of their employed method and the smaller number of their studied arrangements. Also note the asymmetry in the radial extent of the sub-regions corresponding to positive and negative Φ values, where in general the range is wider for $\Phi < 0^\circ$. This is due to a slight asymmetry in the wake of the upstream turbine, which has also been observed in previous experimental and numerical studies for isolated solo VAWTs [27,28]. The mentioned slight symmetry is further discussed in Section 6.1. Elaboration of the flow physics is presented in Section 5.

(iii) *Minimal interaction region:* The remaining area in the test matrix, which was not categorized in the wake and optimal regions, is defined as a minimal interaction region in which $0.95 \leq C_P^{TurbII}/C_P^{Solo} < 1.025$. Within this region, the mutual influence of the two turbines is very limited.

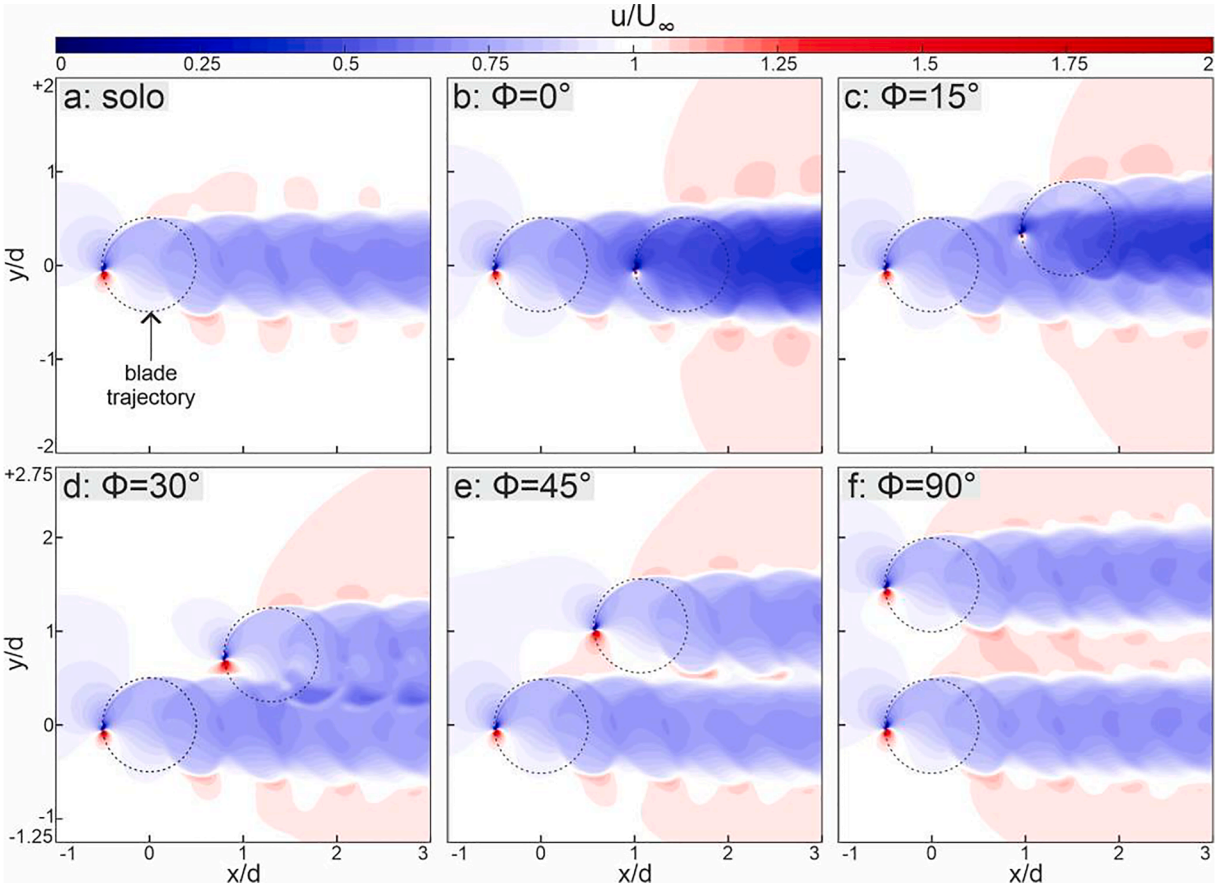

Fig. 11. Normalized instantaneous streamwise velocity (with blades positioned at θ = 90°) for solo rotor and double rotor arrangements with R = 1.5d for different relative angles.

4.2.3. Overall array

Since the variations of C_P^{TurbI} with Φ and R are substantially less than that of the C_P^{TurbII}, the downstream turbine has a dominant impact on the overall trend of $C_P^{overall}$. Therefore, the trend observed for $C_P^{overall}$ is somewhat similar to that of the downstream turbine, although there are some small differences between the two in the optimal region.

By placing the two rotors in the following relative spacings, a significant drop ($C_P^{TurbII}/C_P^{Solo} < 0.95$) in the $C_P^{overall}$ is observed due to the wake interactions of the turbines with a minimum value of $C_P^{Overall}/C_P^{Solo} \cong 0.68$ at $\Phi = 0^\circ$ with $R/d \leq 5$.

- $-5^\circ \leq \Phi \leq +5^\circ$ with $R/d \leq 10$;
- $-10^\circ \leq \Phi < -5^\circ$, $+5^\circ < \Phi \leq +10^\circ$ with $R/d \leq 3$;
- $-15^\circ \leq \Phi < -10^\circ$, $+10^\circ < \Phi \leq +15^\circ$ with $R/d \leq 2.25$;
- $-30^\circ \leq \Phi < -15^\circ$, $+15^\circ < \Phi \leq +30^\circ$ with $R/d \leq 1.5$;

Placing the rotors in the following relative spacings leads to a slight increase in $C_P^{overall}$ compared to C_P^{Solo}, which is due to the synergic interactions between the turbines, detailed in Section 5. The maximum increment of $C_P^{overall}$ compared to C_P^{Solo} in this region is + 1.8%.

- $\Phi = -45^\circ$ with $2.25 \leq R/d \leq 3$; $\Phi = +45^\circ$ with $1.5 \leq R/d \leq 3$;
- $\pm 60^\circ \leq \Phi < \pm 90^\circ$ with $1.25 \leq R/d \leq 3$;

Dashed lines included in Fig. 8c roughly represent the regions mentioned above. For arrangements where the relative spacing of the two rotors is not within the aforementioned ranges, the mutual influence of the rotors is limited and $C_P^{overall}$ is comparable to an isolated solo turbine.

The trends observed for $C_P^{overall}$ are very promising for arrangements of VAWTs in close proximity, where the overall power coefficient of the double rotor array would still be equal to or slightly higher than that of an isolated solo rotor. This grants the opportunity for optimal wind farms with higher power output per unit land area compared to existing HAWT wind farms [4], minimum negative wake interactions and even positive wake interactions contributing to higher performance of the farm.

The discussions so far have considered a fixed relative spacing for the array. While R is a fixed value, Φ typically varies due to the inevitable variations in the wind direction. Therefore, an analysis of $C_P^{overall}$ averaged over all wind directions is also very instructive. Table 7 presents the normalized C_P values for the two rotors as well as the overall array, averaged over Φ. The minimum value for the array is 88% of the $C_P^{Solo,}$ corresponding to the smallest relative distance of R/d = 1.25. By increasing the R, this value grows up to 93% and 97% of the C_P^{Solo} for R/d = 3 and 10, respectively.

The limited average drop of maximum 12% in $C_P^{Overall}$ considering the very small relative distance of R/d = 1.25, and 7% at R/d = 3, is very promising as it reveals the high potential of compact VAWT farms with $C_P^{Overall}$, averaged over all Φ values, comparable to an isolated solo turbine. This allows for a larger number of rotors densely packed within a given area, which in turn, leads to higher power density per farm.

Note that averaging over all Φ values is not an unrealistic assumption for regions with frequent change in wind direction and nearly equal probability of wind blowing from all directions, e.g., urban areas [51,52]. On the other hand, for sites with the wind blowing over a

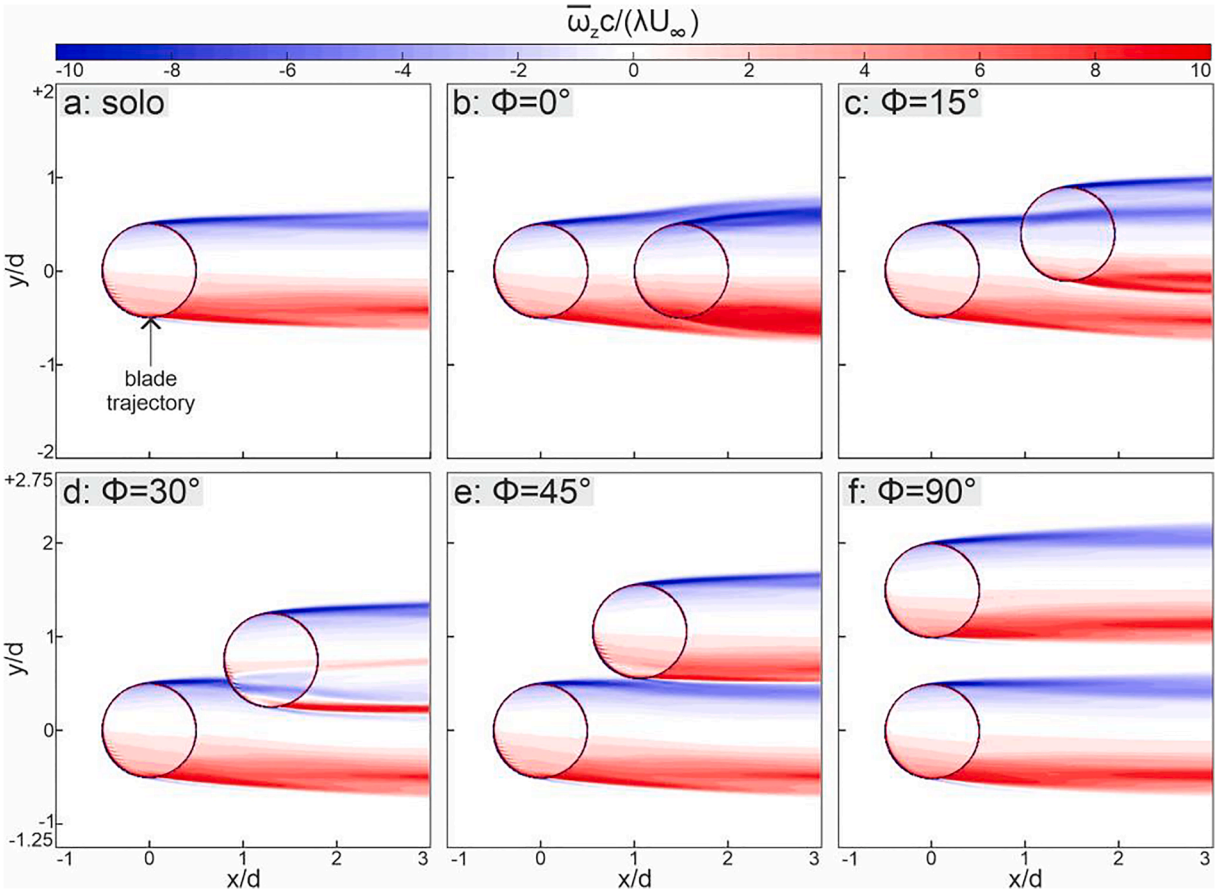

Fig. 12. Normalized time-averaged (over one turbine revolution) Z-vorticity for solo rotor and double rotor arrangements with R = 1.5d for different relative angles.

limited range of directions, the arrangement can be designed according to the dominant wind direction and an estimate of $C_P^{Overall}$ can be made only by averaging over that specific range of Φ.

5. Aerodynamics

5.1. Near wake and blade aerodynamics

To elucidate the underlying physics contributing to the individual and overall power performance enhancement/reduction of the double rotor VAWT arrangements, five selected arrangements are further investigated, all with a relative distance of R/d = 1.5 at different Φ values of 0°, +15°, +30°, +45° and + 90°. These five selected arrangements cover the three regions identified in Section 4.2.2 for the downstream turbine, where Φ = 0°, +15°, and + 30° correspond to the wake region, Φ = +45° is in the optimal region and Φ = +90° is in the minimal interaction region. Table 8 details the C_P values of the selected arrangements.

Fig. 9 illustrates the instantaneous momentum coefficient (C_m) for the selected arrangements, presented in Table 8, in comparison to that of the solo turbine. Figs. 10 and 11 depict the normalized time-averaged (over one turbine revolution) and instantaneous streamwise velocity. Figs. 12 and 13 illustrate the normalized time-averaged (over one turbine revolution) and instantaneous Z-vorticity.

Regarding the upstream turbine, C_m values are very close to the solo turbine with some differences in the second half of the revolution, approximately around 230° < θ < 300° (Fig. 9a). This is due to the induction field of the downstream turbine, which results in a reduction in the incoming flow velocity experienced by the upstream turbine. The largest reduction in C_m values corresponds to Φ = 0° and the magnitude of the reduction lessens by increasing Φ towards 45° (Fig. 9a). This is consistent with the trend observed for C_P values in Fig. 7b and Table 8.

Regarding the downstream turbine, noticeable differences are observed between C_m values of different relative angles:

- At Φ = 0°: C_m values are significantly lower than that of the solo turbine throughout the turbine revolution (Fig. 9b), due to the downstream rotor being fully placed in the low-velocity wake region of the upstream rotor, see Figs. 10b and 11b.
- At Φ = 15° and 30°, the downstream rotor is partially located in the wake of the upstream one, see Figs. 10c-d and 11c-d, which results in strong blade-wake interactions, see Fig. 13c-d. This is also reflected in the C_m plots in the form of a sudden drop occurring at azimuthal angles where the blade enters the low-velocity wake region. This corresponds to θ ≈ 65° and 100° for the relative spacings of Φ = 15° and 30°, respectively.
- At Φ = 45°, the downstream rotor is placed just outside the wake of the upstream rotor, see Figs. 11e and 13e. This creates a narrow passage bounded by the two rotor wakes on both sides, which inevitably contracts the flow streamlines. The analysis of the instantaneous streamwise velocity field, with blades positioned at θ = 90° shown in Fig. 11e, reveals that a region of high velocity is created in this passage through which the blades pass and thus generate higher C_m values, see Fig. 9b. This is found to be the contributing aerodynamic factor for higher C_P^{TurbII} values within the optimal region, discussed in Section 4.2.2, which for this case, results

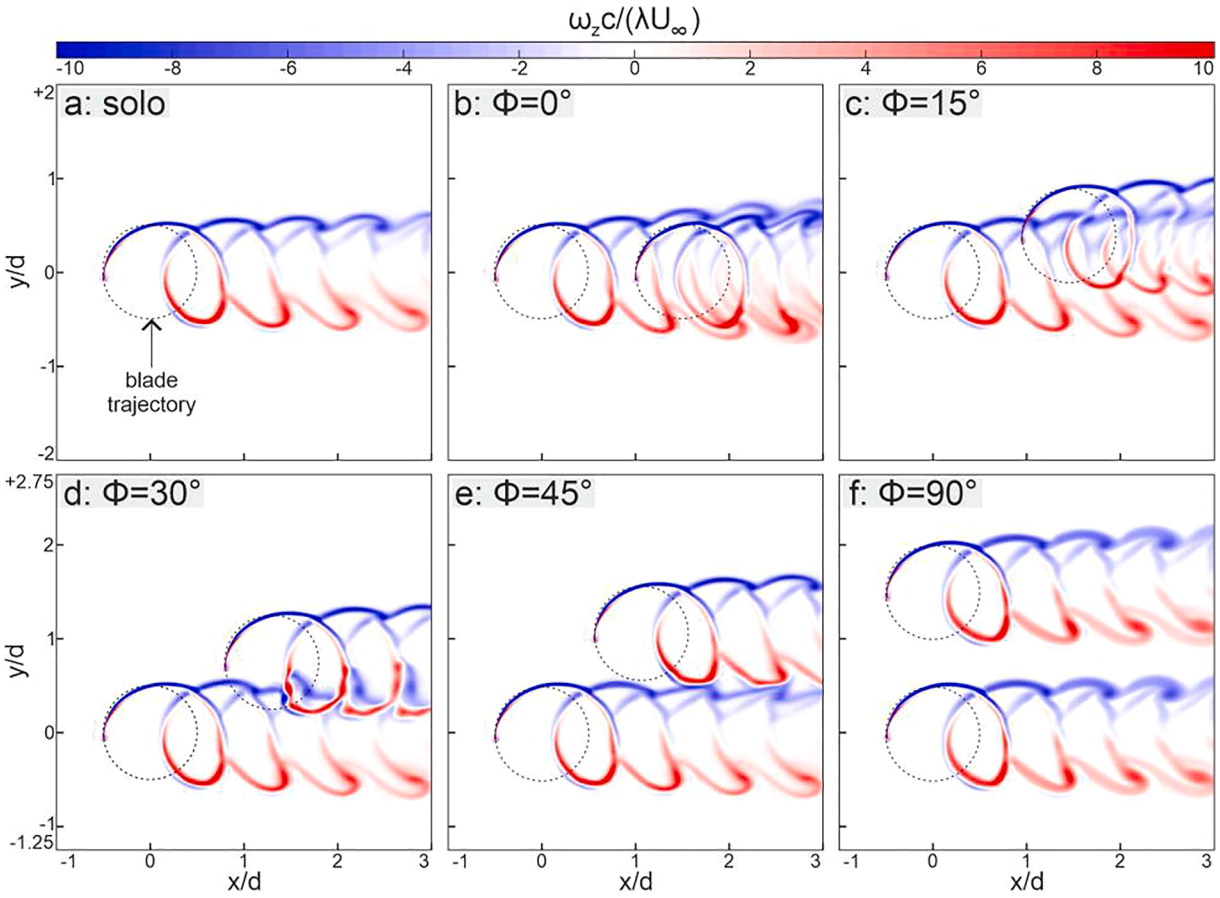

Fig. 13. Normalized instantaneous Z-vorticity (with blades positioned at θ = 90°) for solo rotor and double rotor arrangements with R = 1.5d for different relative angles.

in a 4.7% increase compared to C_P^{solo}. Comparison of the time-averaged and instantaneous vorticity fields of the two rotors at Φ = 45° (Figs. 12e and 13e) against Φ = 90° (Fig. 12f and 13f) also suggests that the two rotors' wakes are still not fully decoupled and some interaction is still present between the bounding vortices. This could also be another contributing factor to the power performance increase of the downstream turbine. Further analysis of this hypothesis using more advanced scale-resolving simulations or high spatiotemporal resolution experimental measurements is needed.

- At Φ = 90°, the wake regions of the two rotors are far enough, even at R/d = 1.5, to be decoupled and minimal aerodynamic interaction between the two rotors happens, see Figs. 12f and 13f. Although Fig. 10f and 11f still show a local region of comparatively high velocity in the passage between the two rotor wakes, the contribution to the C_P^{TurbII} values is limited to 1.4% in comparison to C_P^{solo}.

5.2. Far wake

The wake length of the selected arrangements, see Table 8, is compared to that of the solo turbine in Fig. 14. The wake length here is defined as the streamwise distance along the centerline (y/d = 0) between the upstream rotor center and the point in the wake where $u/U_\infty = 0.97$. The overall wake length of the array for the selected cases with R/d = 1.5 is found to be weakly sensitive to the relative angle of the turbines and is comparable to that of an isolated solo turbine with a maximum and minimum difference of 9.3% and 3.1% corresponding to Φ = 0° and 90°, respectively.

Fig. 15 depicts the contour plots of the normalized instantaneous lateral velocity and Z-vorticity in the far field for the selected arrangements, given in Table 8. Fig. 16 shows the normalized instantaneous lateral velocity zooming in the near field, where the blade traces are indicated with dashed black lines. The following observations are made:

- Solo rotor: the turbine wake breaks up at a downstream distance of x/d ≈ 15–17 and relatively weak vortices are formed in order to diffuse the turbine wake into the freestream condition (Fig. 15a and g).
- Φ = 0°: The wake is found to break up much earlier, compared to the solo rotor, at a downstream distance of x/d ≈ 8. Following that, vortices with significantly higher strength, compared to the solo rotor, are formed, which results in an oscillating wake tail at x/d ≈ 10–15 (Fig. 14b). The comparatively early wake break-up is due to the higher instabilities caused by the strong wake interactions of the two tandem rotors. Fig. 16b shows that the blade traces in the near wake (illustrated by dashed lines) are nearly 35% closer in the Φ = 0° arrangement compared to the solo rotor. This adjacency leads to higher amplification of the instabilities in the wake, which eventually results in the discussed early wake break up. Due to this early wake break-up, strong vortices are formed as a mechanism so that the flow can diffuse to the freestream flow characteristics (Fig. 15b and h).
- Φ = 15°, 30° and 45°: By increasing the relative angle between the two turbines, the wake break-up point moves further downstream. For the Φ = 15°, 30° and 45° arrangements, wake break-up happens

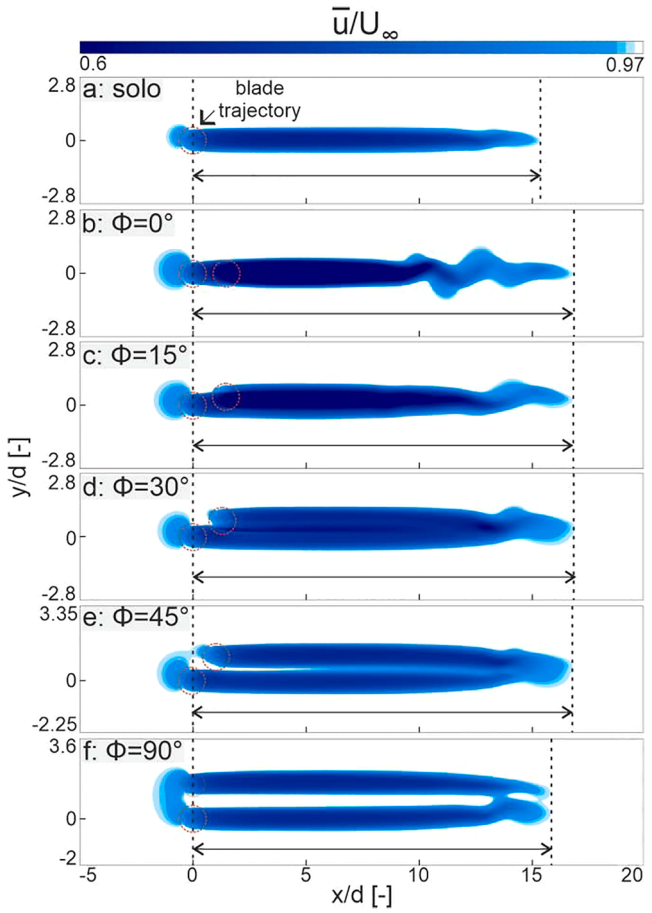

Fig. 14. Contour plots of the normalized time-averaged (over one turbine revolution) streamwise velocity, employed to identify the wake length of the selected arrangements compared to the solo turbine (R = 1.5d).

at a downstream distance of x/d ≈ 9, 13 and 14, respectively. Consequently, in these arrangements, weaker vortices are formed compared to the Φ = 0° arrangement. The later wake break-up for higher Φ values, compared to Φ = 0°, is due to the decrease in the wake interactions by increasing Φ, which results in less amplification of the wake instabilities. The reduction in the amplification of the wake instabilities for higher Φ can also be inferred from the larger distance between the blade traces for higher values of Φ, see Fig. 16b-–d. For the Φ = 30° and 45° arrangements, the distance between the blade traces in the wake is 50% and 65% higher than that of Φ = 0°, respectively.

- Φ = 90°: Compared to the solo rotor, the wake break-up of the two side-by-side rotors with a relative distance of 1.5d happens at a smaller downstream distance of x/d ∼ 14. Consistent with the comparatively earlier wake break-up, the strength of the formed vortices are higher than that of the solo rotor. This suggests that at a relative distance of R = 1.5d, there remains some wake interactions between the two rotors in the far wake (Fig. 15f and l).

6. Discussion

6.1. Unequal C_P values for +/− relative angles

Detailed analysis of the results shows that, for a given relative distance, the C_P^{TurbII} values for the arrangements with relative angles of the same value and different signs are not equal. This can be detected in Fig. 6a–d, Fig. 7a–d and to a lesser extent in Fig. 8b. To clarify, two arrangements with the same relative distance of R = 1.5d at Φ = +15° and −15° are further investigated. C_P^{TurbII} values for Φ = +15° and −15° are 0.1886 and 0.2006, respectively, corresponding to 0.68 and 0.7 of the C_P^{Solo}. The relative difference between the two is about 6%.

Fig. 17 illustrates the normalized time-averaged streamwise velocity of the two arrangements. Fig. 18 shows the instantaneous momentum coefficient (C_m) of the downstream turbine.

For the case of Φ = +15° arrangement, the region where the downstream turbine is located outside of the upstream turbine wake corresponds to a large portion of the windward side of the revolution (approximately 305° ≤ θ < 65°, Fig. 17a), while for the Φ = −15° arrangement, this corresponds to most of the leeward side of the revolution cycle (approximately 110° ≤ θ < 240°, Fig. 17b). This is also evident in Fig. 18 by comparing the C_m plots of the two arrangements at identical θ as where the downstream turbine is out of the upstream turbine wake, it has comparatively higher C_m values. Therefore, different parts of the revolution cycle of the downstream turbines of the Φ = +15° and −15° arrangements are affected by the wake of the upstream turbine. In addition, asymmetric VAWT wakes in the lateral direction have been reported in previous experimental studies [27,49,50] as well as validated numerical studies [31,32]; meaning that downstream turbines in the Φ = +15° and −15° arrangements are located in different regions of the upstream turbine's wake. Due to these two reasons, the downstream turbines in Φ = +15° and −15° arrangements experience different incoming flow velocities in the wake of the upstream turbine.

The abovementioned reasons explain the unequal C_P values for arrangements with equal relative distances but relative angles of the same value and different signs. However, since this inequality is caused by the wake of the upstream turbine, by increasing the relative angle to Φ ≥ 60° in which the wakes of the two turbines are mostly separated and in arrangements with R ≥ 5d where the wake effects are minimal, the inequality fades away (Fig. 6f–h and Fig. 7e–f).

6.2. Limitations of the study

The present study uses 2D CFD simulations, which come with inherent shortcomings compared to a full 3D analysis. Most importantly, the recovery rate of the turbine wakes in 2D simulations, especially in the far-wake region, is usually lower than that predicted in full 3D simulations. This is due to the lack of span-wise mean flow and vertical turbulent mixing in 2D simulations. However, this shortcoming is thought not to have a significant impact on the local blade aerodynamics and the near wake flow. Consequently, the power performance analysis of arrangements with a small relative distance corresponding to turbines placed in close proximity, would be minimally affected [5]. 3D analysis of the performance of double rotor arrangements, nevertheless, can be of interest in future research.

The Reynolds number (Re) and tip speed ratio (λ) of interest in this study correspond to the optimal operational conditions of the particular simulated turbines and the regime of interest for urban VAWT wind energy harvesting. Generalizing the findings to cover higher Re and λ, experienced in large-scale offshore VAWT wind farms, must be carried out cautiously, and further research is required for that purpose.

The relative rotation direction of the turbines and their relative phase difference are important parameters, which influence the aerodynamics and power performance of the rotors. The current study investigates two co-rotating VAWTs with similar azimuthal starting points (i.e., no phase difference). Therefore, investigation of the effects of rotation direction (i.e., counter-rotating turbines) and phase lag (i.e., turbines with different azimuthal starting points) is proposed.

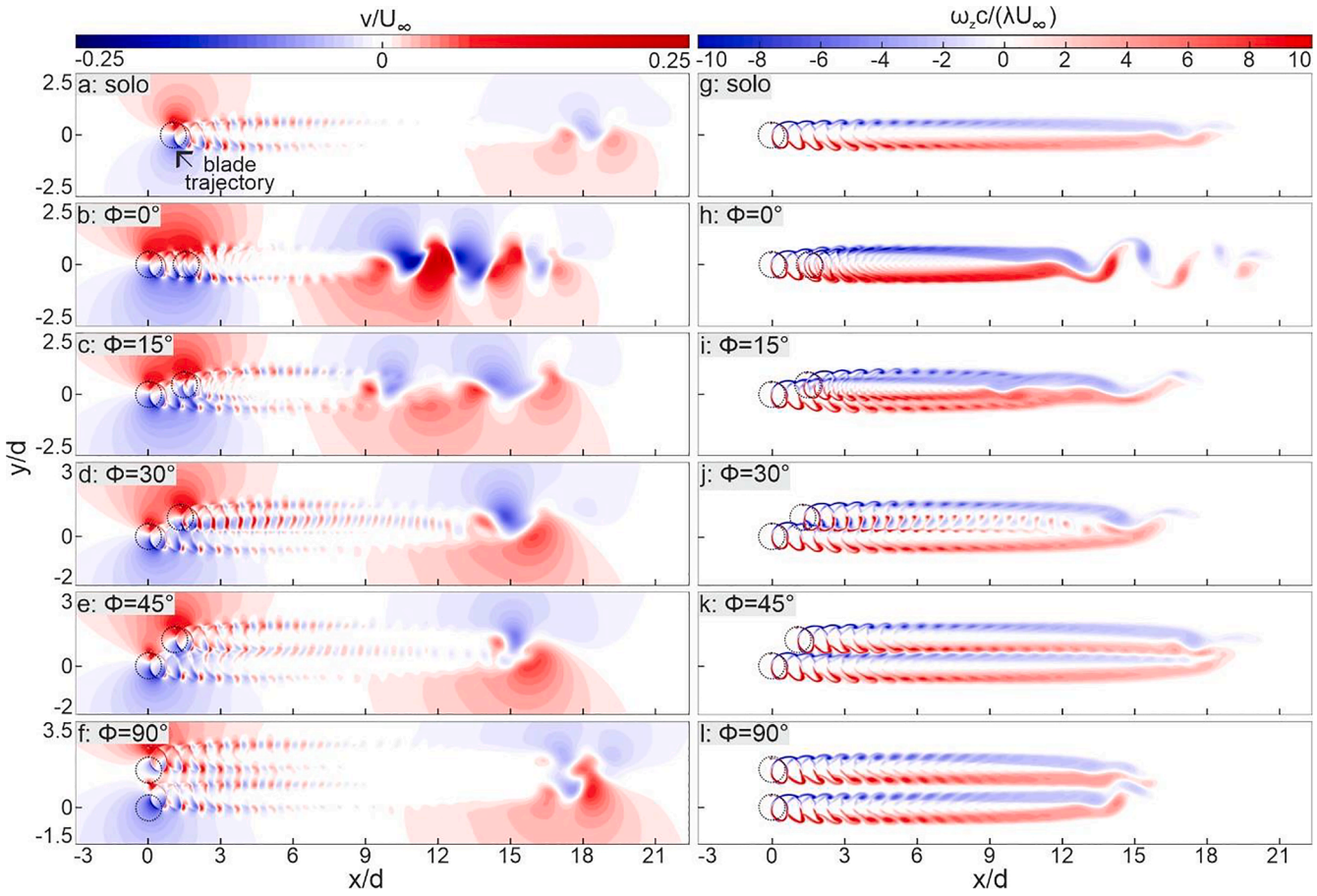

Fig. 15. (a–f) Normalized instantaneous lateral velocity and (g–l) Z-vorticity (with blades positioned at $\theta = 0°$) for the solo rotor and double rotor arrangements with R = 1.5d at different relative angles.

7. Conclusions

High-fidelity URANS simulations, validated with experimental data, are carried out to systematically investigate the effect of relative spacing (i.e., relative distance and relative angle), on the individual and overall power performance of two co-rotating, co-phase turbines in a double rotor VAWT arrangement. The study covers a wide range of values for both relative distance ($1.25d \leq R \leq 10d$) and relative angle ($-90° \leq \Phi \leq +90°$).

The main conclusions are as follows:2

- Regarding the upstream turbine:
  - The power coefficient drops to a minimum of 90% of an isolated solo turbine (C_P^{Solo}) for $R/d \leq 2.25$ at $-45° \leq \Phi \leq +30°$. The drop is due to the upstream induction of the downstream turbine (TurbII).
  - Outside the aforementioned region, the impact of TurbII on C_P^{TurbI} is limited to <5% for $R/d < 5$ and below 2% for $R/d \geq 5$.

- Regarding the downstream turbine:
  - The following 3 regions are identified for TurbII: (a) wake region, $C_P^{TurbII}/C_P^{Solo} < 0.95$; (b) optimal region, $C_P^{TurbII}/C_P^{Solo} \geq 1.025$; and (c) minimal interaction region, $0.95 \leq C_P^{TurbII}/C_P^{Solo} < 1.025$.
  - In the wake region, significant wake interactions are present between the two rotors. C_P^{TurbII} drops to a minimum value of 39.5% of C_P^{Solo} at $R/d = 5$ and $\Phi = 0°$. The region expands to $R/d = 10$ for $-5° \leq \Phi \leq +5°$, to $R/d = 3$ for $-15° \leq \Phi < -5°$, $+5° < \Phi \leq +15°$, and to $R/d = 1.5$ for $-30° \leq \Phi < -15°$, $+15° < \Phi \leq +30°$.
  - In the optimal region, the downstream rotor is found to benefit from a high-velocity region created due to the formation of an in-between passage for the two adjacent rotors. As a result, C_P^{TurbII} grows up to 5.2% higher than C_P^{Solo}.
  - In the minimal interaction region, the two rotors have inconsiderable mutual interaction, and each operates comparable to an isolated solo rotor.

- Regarding the overall array:
  - Optimal relative spacing is found that yields $C_P^{overall}$ slightly higher than C_P^{Solo}. This region corresponds to the following relative spacings: $\Phi = -45°$ with $2.25 \leq R/d \leq 3$; $\Phi = +45°$ with $1.5 \leq R/d \leq 3$; and $\pm 60° \leq \Phi < \pm 90°$ with $1.25 \leq R/d \leq 3$. In this region, a maximum increment of 1.8% is achieved for the arrangement with $R/d = 1.25$ and $\Phi = +75$.
  - For the relative spacings where the downstream rotor is located in the wake region, a significant drop in $C_P^{overall}$ is observed due to the wake interactions of the turbines with a minimum value of $C_P^{Overall}/C_P^{Solo} \cong 0.68$ corresponding to $\Phi = 0°$ with $R/d \leq 5$.
  - By placing the two rotors in relative spacings other than the aforementioned two ranges, $C_P^{Overall}$ is comparable to C_P^{Solo}.
  - Double VAWTs placed side by side operate almost decoupled with minimum aerodynamic interactions, even at relative distances as small as $R/d = 1.5$.
  - Considering the inevitable variations of wind direction (and Φ), the $C_P^{overall}$ of the array averaged over all Φ values is also studied. For

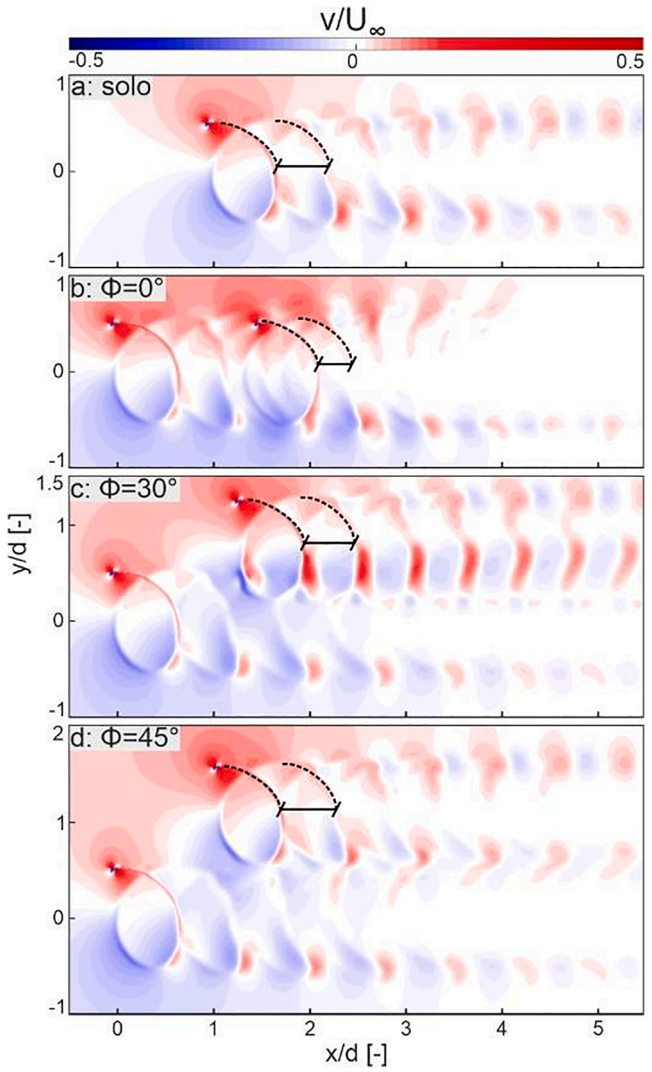

Fig. 16. Normalized instantaneous lateral velocity (with blades positioned at θ = 0°) in the near wake of the turbines for solo rotor and double rotor arrangements with R = 1.5d with different relative angles. Blade traces are indicated with dashed black lines.

R/d ≤ 1.75, this is nearly 90% of C_P^{Solo}, confirming the high potential for compact VAWT farms irrespective of wind direction variations.

Current findings underline and help better understand the importance of the effect of turbines' arrangement on their individual and overall power performance in VAWT arrays. The results confirm the great potential for compact arrays of VAWTs with high power densities. As an example, double rotor arrays with small relative distances of R/d ≤ 3 and a wide range of relative angles can yield $C_P^{Overall} \geq C_P^{Solo}$.

This potential higher power density is especially of great value in dense urban areas where there is a shortage of available space for the installation of wind energy harvesting systems. Present results can also be used as a starting point towards layout design and optimization of VAWT farms and in support of more widespread wind energy harvesting, especially in urban areas.

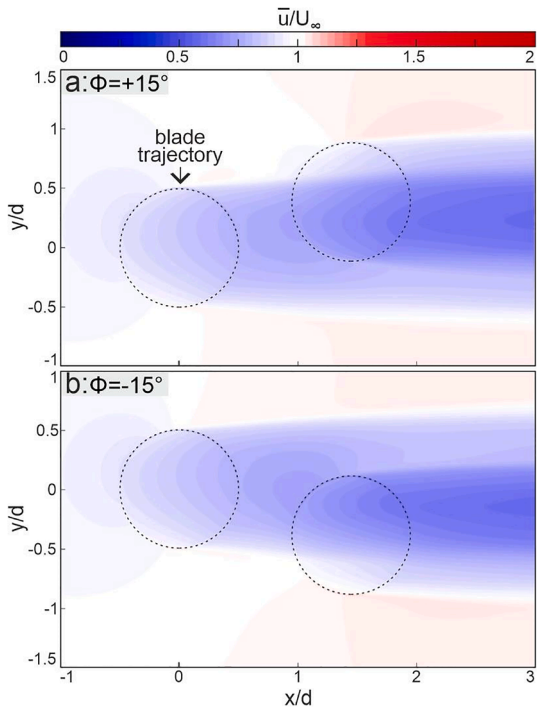

Fig. 17. Normalized time-averaged (over one turbine revolution) streamwise velocity for symmetric double rotor arrangements with a relative distance of R = 1.5d and relative angles of (a) Φ = +15° and (b) Φ = −15°.

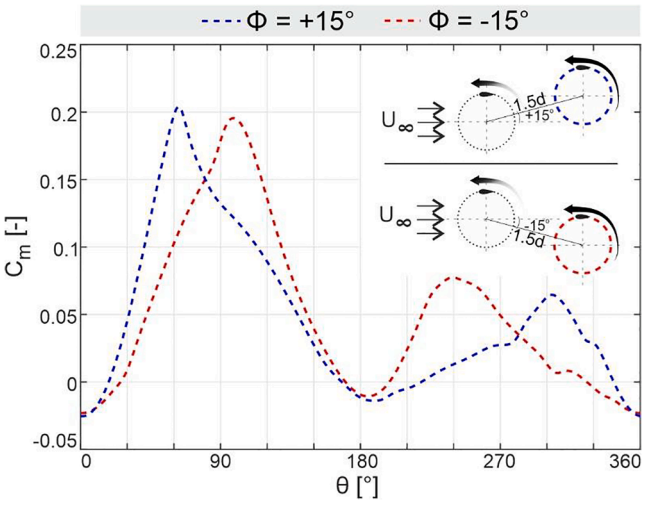

Fig. 18. Instantaneous momentum coefficient (C_m) for the downstream turbines for symmetric double rotor arrangements with a relative distance of R = 1.5d and relative angles of Φ = +15° and −15°.

CRediT authorship contribution statement

Sadra Sahebzadeh: Conceptualization, Methodology, Software, Validation, Formal analysis, Investigation, Data curation, Writing-original draft, Writing-review and editing, Visualization, Funding acquisition. **Abdolrahim Rezaeih:** Conceptualization, Methodology, Software, Validation, Resources, Writing-original draft, Writing-review and editing, Visualization, Supervision. **Hamid Montazeri:** Conceptualization, Methodology, Writing-review and editing, Supervision, Project administration.

Declaration of Competing Interest

The authors declare that they have no known competing financial interests or personal relationships that could have appeared to influence the work reported in this paper.

Acknowledgements

This work was sponsored by NWO Exacte Wetenschappen (Physical Sciences) for the use of supercomputer facilities, with financial support from the Nederlandse Organisatie voor Wetenschappelijk Onderzoek (Netherlands Organization for Scientific Research, NWO). The authors would also like to acknowledge the partnership with ANSYS CFD. The 2nd author is currently a postdoctoral fellow of the Research Foundation – Flanders (FWO) and is grateful for its financial support (project FWO 12ZP520N).

References

[1] González-Longatt F, Wall P, Terzija V. Wake effect in wind farm performance: Steady-state and dynamic behavior. Renewable Energy 2012;39(1):329–38.
[2] Bartl J, Pierella F, Sætrana L. Wake measurements behind an array of two model wind turbines. Energy Procedia 2012;24:305–12.
[3] Shakoor R, Hassan MY, Raheem A, Wu Y-K. Wake effect modeling: A review of wind farm layout optimization using Jensen's model. Renew Sustain Energy Rev 2016;58:1048–59.
[4] Dabiri JO. Potential order-of-magnitude enhancement of wind farm power density via counter-rotating vertical-axis wind turbine arrays. J Renew Sustain Energy 2011;3(4):043104. https://doi.org/10.1063/1.3608170.
[5] Zanforlin S, Nishino T. Fluid dynamic mechanisms of enhanced power generation by closely spaced vertical axis wind turbines. Renew Energy 2016;99:1213–26.
[6] Brownstein ID, Wei NJ, Dabiri JO. Aerodynamically Interacting Vertical-Axis Wind Turbines: Performance Enhancement and Three-Dimensional Flow. Energies 2019; 12(14):2724.
[7] Chowdhury S, Zhang J, Messac A, Castillo L. Unrestricted wind farm layout optimization (UWFLO): Investigating key factors influencing the maximum power generation. Renew Energy 2012;38(1):16–30.
[8] Yang Li, Peng R, Li G, Lee C-G. Operations management of wind farms integrating multiple impacts of wind conditions and resource constraints. Energy Convers Manage 2020;205:112162. https://doi.org/10.1016/j.enconman.2019.112162.
[9] Vermeer LJ, Sørensen JN, Crespo A. Wind turbine wake aerodynamics. Prog Aerosp Sci 2003;39(6-7):467–510.
[10] Sanderse B. Aerodynamics of wind turbine wakes-literature review. ECN 2009.
[11] Sørensen JN. Wind turbine wakes and wind farm aerodynamics. Wind Energy Syst 2011:112–29.
[12] Mehta D, van Zuijlen AH, Koren B, Holierhoek JG, Bijl H. Large Eddy Simulation of wind farm aerodynamics: A review. J Wind Eng Ind Aerodyn 2014;133:1–17.
[13] Stevens RJAM, Meneveau C. Flow structure and turbulence in wind farms. Annu. Rev. Fluid Mech. 2017;49(1):311–39.
[14] Porté-Agel F, Bastankhah M, Shamsoddin S. Wind-turbine and wind-farm flows: A review. Boundary-Layer Meteorol 2020;174(1):1–59.
[15] Brownstein ID, Kinzel M, Dabiri JO. Performance enhancement of downstream vertical-axis wind turbines. J Renewable Sustainable Energy 2016;8(5):053306. https://doi.org/10.1063/1.4964311.
[16] Ahmadi-Baloutaki M, Carriveau R, Ting D-K. A wind tunnel study on the aerodynamic interaction of vertical axis wind turbines in array configurations. Renewable Energy 2016;96:904–13.
[17] Lam HF, Peng HY. Measurements of the wake characteristics of co- and counter-rotating twin H-rotor vertical axis wind turbines. Energy 2017;131:13–26.
[18] Chen W-H, Chen C-Y, Huang C-Y, Hwang C-J. Power output analysis and optimization of two straight-bladed vertical-axis wind turbines. Appl Energy 2017; 185:223–32.
[19] De TD, Ferreira C, Li A, Paulsen US, Madsen HA. Towards the understanding of vertical-axis wind turbines in double-rotor configuration. J Phys Conf Ser 2018; 1037(2):22015.
[20] Barnes A, Hughes B. Determining the impact of VAWT farm configurations on power output. Renew Energy 2019;143:1111–20.
[21] Alexander AS, Santhanakrishnan A. Mechanisms of power augmentation in two side-by-side vertical axis wind turbines. Renew Energy 2020;148:600–10.
[22] Peng HY, Han ZD, Liu HJ, Lin K, Lam HF. Assessment and optimization of the power performance of twin vertical axis wind turbines via numerical simulations. Renew Energy 2020;147:43–54.
[23] Whittlesey RW, Liska S, Dabiri JO. Fish schooling as a basis for vertical axis wind turbine farm design. Bioinspir Biomim 2010;5(3):035005. https://doi.org/10.1088/1748-3182/5/3/035005.
[24] Bremseth J, Duraisamy K. Computational analysis of vertical axis wind turbine arrays. Theor Comput Fluid Dyn 2016;30(5):387–401.
[25] Cetinay H, Kuipers FA, Guven AN. Optimal siting and sizing of wind farms. Renew Energy 2017;101:51–8.
[26] Rezaeiha A, Montazeri H, Blocken B. Characterization of aerodynamic performance of vertical axis wind turbines: Impact of operational parameters. Energy Convers Manag 2018;169:45–77.
[27] Tescione G, Ragni D, He C, Simão Ferreira CJ, van Bussel GJW. Near wake flow analysis of a vertical axis wind turbine by stereoscopic particle image velocimetry. Renewable Energy 2014;70:47–61.
[28] Rezaeiha A, Montazeri H, Blocken B. Towards optimal aerodynamic design of vertical axis wind turbines: Impact of solidity and number of blades. Energy 2018; 165:1129–48.
[29] Rezaeiha A, Kalkman I, Montazeri H, Blocken B. Effect of the shaft on the aerodynamic performance of urban vertical axis wind turbines. Energy Convers Manage 2017;149:616–30.
[30] Tummala A, Velamati RK, Sinha DK, Indraja V, Krishna VH. A review on small scale wind turbines. Renew Sustain Energy Rev 2016;56:1351–71.
[31] Rezaeiha A, Kalkman I, Blocken B. CFD simulation of a vertical axis wind turbine operating at a moderate tip speed ratio: Guidelines for minimum domain size and azimuthal increment. Renewable Energy 2017;107:373–85.
[32] Rezaeiha A, Montazeri H, Blocken B. Towards accurate CFD simulations of vertical axis wind turbines at different tip speed ratios and solidities: Guidelines for azimuthal increment, domain size and convergence. Energy Convers Manage 2018; 156:301–16.
[33] Fluent A. Theory guide. PA, USA: Ansys Inc Canonsburg; 2015.
[34] Patankar SV, Spalding DB. A calculation procedure for heat, mass and momentum transfer in three-dimensional parabolic flows. Int J Heat Mass Transf 1972;15(10): 1787–806.
[35] Patankar SV. Numerical heat transfer and fluid flow. Washington DC: Hemisph Publ Corp; 1980.
[36] Gottlieb S, Shu C-W. Total variation diminishing Runge-Kutta schemes. Math Comp 1998;67(221):73–85.
[37] Menter FR, Langtry RB, Likki SR, Suzen YB, Huang PG, Volker S. A correlation-based transition model using local variables-Part I: Model formulation. J. Turbomach. 2006;128(3):413. https://doi.org/10.1115/1.2184352.
[38] Wilcox DC. Turbulence modeling for CFD, vol. 2. CA: DCW industries La Canada; 1998.
[39] Menter FR. Two-equation eddy-viscosity turbulence models for engineering applications. AIAA J 1994;32(8):1598–605.
[40] Kato M. The modelling of turbulent flow around stationary and vibrating square cylinders. Turbul Shear Flow 1993;1:10–4.
[41] Spalart PR, Shur M. On the sensitization of turbulence models to rotation and curvature. Aerosp Sci Technol 1997;1(5):297–302.
[42] Steijl R, Barakos G. Sliding mesh algorithm for CFD analysis of helicopter rotor-fuselage aerodynamics. Int J Numer Meth Fluids 2008;58(5):527–49.
[43] Blocken B, Stathopoulos T, Carmeliet J. Wind environmental conditions in passages between two long narrow perpendicular buildings. J Aerosp Eng 2008;21(4): 280–7.
[44] Blocken B, Stathopoulos T, Carmeliet J. CFD simulation of the atmospheric boundary layer: wall function problems. Atmos Environ 2007;41(2):238–52.
[45] Blocken B, Carmeliet J, Stathopoulos T. CFD evaluation of wind speed conditions in passages between parallel buildings–effect of wall-function roughness modifications for the atmospheric boundary layer flow. J Wind Eng Ind Aerodyn 2007;95(9-11):941–62.
[46] Rezaeiha A, Montazeri H, Blocken B. CFD analysis of dynamic stall on vertical axis wind turbines using Scale-Adaptive Simulation (SAS): Comparison against URANS and hybrid RANS/LES. Energy Convers Manage 2019;196:1282–98.
[47] Rezaeiha A, Montazeri H, Blocken B. On the accuracy of turbulence models for CFD simulations of vertical axis wind turbines. Energy 2019;180:838–57.
[48] Roache PJ. Quantification of uncertainty in computational fluid dynamics. Annu Rev Fluid Mech 1997;29(1):123–60.
[49] Simão Ferreira C, van Kuik G, van Bussel G, Scarano F. Visualization by PIV of dynamic stall on a vertical axis wind turbine. Exp Fluids 2009;46(1):97–108.
[50] Raciti Castelli M, Englaro A, Benini E. The Darrieus wind turbine: Proposal for a new performance prediction model based on CFD. Energy 2011;36(8):4919–34.
[51] Sunderland KM, Mills G, Conlon MF. Estimating the wind resource in an urban area: A case study of micro-wind generation potential in Dublin, Ireland. J Wind Eng Ind Aerodyn 2013;118:44–53.
[52] Rezaeiha A, Montazeri H, Blocken B. A framework for preliminary large-scale urban wind energy potential assessment: Roof-mounted wind turbines. Energy Convers Manage 2020;214:112770. https://doi.org/10.1016/j.enconman.2020.112770.